Natural Resources Canada | Ressources naturelles Canada

GEOLOGICAL SURVEY OF CANADA
OPEN FILE 8867

Alteration and ore assemblages of the LaRonde Zone 5 (LZ5) deposit and Ellison mineralized zones, Doyon-Bousquet-LaRonde mining camp, Abitibi, Quebec

E. Boily-Auclair, P. Mercier-Langevin, P.-S. Ross, and D. Pitre

2022

Canada

GEOLOGICAL SURVEY OF CANADA
OPEN FILE 8867

Alteration and ore assemblages of the LaRonde Zone 5 (LZ5) deposit and Ellison mineralized zones, Doyon-Bousquet-LaRonde mining camp, Abitibi, Quebec

E. Boily-Auclair[1], P. Mercier-Langevin[2], P.-S. Ross[1], and D. Pitre[3]

[1]Institut national de la recherche scientifique – Centre Eau Terre Environnement, 490, rue de la Couronne, Québec, Quebec
[2]Geological Survey of Canada, 490, rue de la Couronne, Québec, Quebec
[3]Agnico Eagle Mines Limited, LaRonde Division, 10200, route de Preissac, Rouyn-Noranda, Quebec

2022

Permanent link: https://doi.org/10.4095/329637

This publication is available for free download through GEOSCAN (https://geoscan.nrcan.gc.ca/).

Recommended citation
Boily-Auclair, E., Mercier-Langevin, P., Ross, P.-S., and Pitre, D., 2022. Alteration and ore assemblages of the LaRonde Zone 5 (LZ5) deposit and Ellison mineralized zones, Doyon-Bousquet-LaRonde mining camp, Abitibi, Quebec; Geological Survey of Canada, Open File 8867, 48 p. https://doi.org/10.4095/329637

Publications in this series have not been edited; they are released as submitted by the author.

Alteration and ore assemblages of the LaRonde Zone 5 (LZ5) deposit and Ellison mineralized zones, Doyon-Bousquet-LaRonde mining camp, Abitibi, Quebec

Emile Boily-Auclair[1*], Patrick Mercier-Langevin[2], Pierre-Simon Ross[1] and David Pitre[3]

[1]Institut national de la recherche scientifique, Centre Eau Terre Environnement, 490 rue de la Couronne, Québec, Quebec G1K 9A9
[2]Geological Survey of Canada, 490 rue de la Couronne, Québec, Quebec G1K 9A9
[3]Agnico Eagle Mines limited, LaRonde Division, 10200 route de Preissac, Rouyn-Noranda, Quebec J0Y 2E0
*Corresponding author email: emile.boily-auclair@geoexplauinternational.com

ABSTRACT

The LaRonde Zone 5 (LZ5) mine is part of the Doyon-Bousquet-LaRonde mining camp and is located in the southern part of the Abitibi greenstone belt in northwestern Quebec. The LZ5 deposit consists of three stacked mineralized corridors: Zone 4, Zone 4.1, and Zone 5. Zones 4 and 4.1 are discontinuous satellite mineralized corridors, whereas Zone 5 represents the main mineralized body.

The mineralized zones of the LZ5 deposit and adjacent Ellison property (Ellison A and B zones) are hosted in the strongly-deformed, 2699-2695 Ma transitional to calc-alkaline, intermediate to felsic, volcanic and volcaniclastic rocks of the Bousquet Formation upper member, which is part of the Blake River Group (2704-2695 Ma). Zones 4, 4.1, and 5 at the LZ5 mine are hosted in intermediate volcanic and volcaniclastic rocks of the Westwood andesitic to rhyodacitic unit (unit 5.1a), which forms the base of the upper member of the Bousquet Formation. The Ellison Zone A is hosted higher up in the stratigraphic sequence within a newly described intermediate volcanic unit. The Ellison Zone B is hosted in felsic volcanic and volcaniclastic rocks of the Westwood feldspar-phyric rhyolite dome (subunit 5.3a-(b)).

Mineralization in all three zones of the LZ5 deposit consists of discordant networks of millimeter- to centimeter-thick pyrite ±chalcopyrite ±sphalerite ±pyrrhotite veins and veinlets (10–20 % of the volume of the rock) and, to a lesser extent, very finely disseminated pyrite and boudinaged veins (≤5 vol. % each) in strongly altered host rocks. Gold commonly occurs as microscopic inclusions in granoblastic pyrite and at the triple junction between recrystallized grains. The veins, stockworks, and disseminations were intensely folded and transposed in the steeply south-dipping, east-west trending S_2 foliation. The vein network is at least partly discordant to the stratigraphy. A distal alteration halo envelops the LZ5 mineralized corridors and consists of a sericite-carbonate-chlorite-feldspar ±biotite assemblage. A proximal sericite-carbonate-chlorite-pyrite-quartz-feldspar-biotite ±epidote alteration assemblage is present within the LZ5 mineralized zones. A local proximal alteration assemblage of sericite-quartz-pyrite is also

locally developed within Zone 4 and Zone 5 of the LZ5 deposit. Mass gains in $Fe_2O_3^{(t)}$ and K_2O, and mass losses in CaO, MgO, Na_2O, and locally SiO_2, are characteristic of the LZ5 alteration zones.

The Ellison zone A and B are similar to LZ5 in terms of style of mineralization, but thin (10–20 cm) veins or bands of semi-massive to massive, finely recrystallized disseminated pyrite (0.1–1 mm) are distinctive. Chalcopyrite and sphalerite are also slightly more abundant in the mineralized corridors of the Ellison property and are usually associated with elevated gold grades. The zones are also slightly richer than at LZ5 in terms of gold and silver content, but narrower and less continuous in general. The Ellison Zone A is characterized by gains in $Fe_2O_3^{(t)}$ and K_2O and losses in CaO, MgO, Na_2O, and SiO_2. Gains in $Fe_2O_3^{(t)}$ and local gains in K_2O, MgO, and MnO, and losses in CO_2, Na_2O, P_2O_5, and SiO_2, characterize the felsic host rocks of the Zone B corridor.

The style of mineralization at LZ5 (pyrite ±chalcopyrite veins and veinlets, ±disseminated pyrite with low base metal content), its setting (i.e. in rocks of intermediate composition at the base of the upper member of the Bousquet Formation), and the geometry of its ore zones (stacked lenses of sulfide veins and veinlets, without massive sulfide lenses) differ from the other major deposits of the Doyon-Bousquet-LaRonde mining camp.

Despite these differences, this study indicates that the LZ5 and Ellison mineralized corridors are of synvolcanic hydrothermal origin and have most likely been formed by convective circulation of seawater below the seafloor. An influx of magmatic fluids from the Mooshla synvolcanic intrusive complex or its parent magma chamber could explain the Au enrichment at LZ5, as has been suggested for other deposits of the camp. Evidence for a pre-deformation synvolcanic mineralization at LZ5 includes ductile deformation and recrystallization of the sulfides, the stacked nature of its ore zones, subconcordant alteration halos that envelop the mineralized corridors, evidence that the mineralized system was already active when the LZ5 lenses were deposited and control on mineralization by primary volcanic features such as the permeability and porosity of the volcanic rocks.

INTRODUCTION

The Abitibi greenstone belt (Fig. 1) represents one of the world's largest and best-preserved Neoarchean terranes (Monecke et al., 2017). It is of significant economic importance for Canada because of the many Au and base metal deposits present in the belt. Its total Au endowment is currently estimated at over 9,375 t Au hosted in different styles of deposits formed at various times during the volcanic, sedimentary, and tectonic evolution of the belt (Dubé and Mercier-Langevin, 2020). In terms of Au production and total Au content, the Doyon-Bousquet-LaRonde (DBL) mining camp ranks fourth in the Abitibi greenstone belt and sixth in the Superior province, with over 790.1 t Au in total past production, current reserves, and measured and indicated resources (Mercier-Langevin et al., 2020).

Three main styles of mineralization are present in the DBL mining camp: 1) Au-rich volcanogenic massive sulfides and Au-rich sulfide veins, stockworks, and

disseminations; 2) epizonal "intrusion-related" sulfide-rich Au ± Cu veins; and 3) shear-hosted sulfide-rich Au-Cu veins (Mercier-Langevin et al., 2017). These contrasting mineralization styles are considered part of an extensive Archean synvolcanic magmatic-hydrothermal system (e.g., Doyon, Bousquet 1 (Zone 3), Bousquet 2-Dumagami, LaRonde Penna, and Westwood; Fig. 2) on which the main phase of deformation and regional metamorphism were superimposed. Numerous DBL camp deposits have been extensively studied over the past few decades (Mercier-Langevin et al., 2017, and references therein). However, the LaRonde Zone 5 (LZ5) deposit and the adjacent Ellison property mineralized zones were not studied in such detail because of a lack of access and material such as drill core samples and whole-rock lithogeochemistry. Therefore, the LZ5 has not been integrated into the most recent and revised metallogenic models for the DBL mining camp (e.g., Dubé et al., 2007, 2014; Mercier-Langevin et al., 2007a-d, 2009, 2017; Yergeau, 2015; Yergeau et al., 2022a, b).

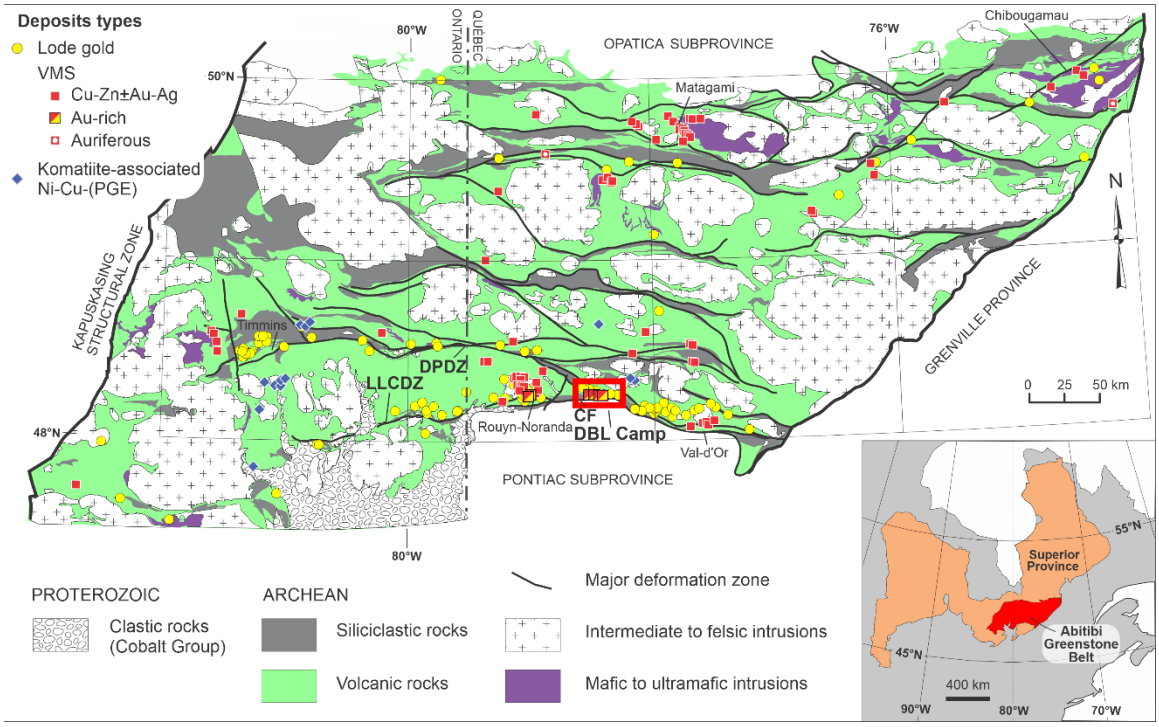

Figure 1. Location and distribution of the major ore deposits found within the Abitibi greenstone belt. Note that the deposits consist mainly of the VMS and Lode-Au types. Abbreviations: LLCDZ = Larder Lake-Cadillac deformation zone. DPDZ = Destor-Porcupine deformation zone. From Mercier-Langevin et al. (2014).

What is now designated as the LaRonde Zone 5 was the first discovery on the Bousquet property in 1937 by Thompson Bousquet Gold Mines Limited. This low-grade mineralized corridor could not be mined economically at the time, but further exploration on the property led to the discovery of the much higher-grade Zone 3 a few tens of meters to the south. The latter was mined by Long Lac Minerals and Barrick Gold Corporation as part of the Bousquet 1 mine, from 1978 to 1996 (Mercier-Langevin et al., 2017, 2021). A small part of Zone 5 was mined at Bousquet 1 from a shallow open pit operation by Barrick Gold, but most of the mineralization underground remained untouched. The Bousquet 1 mine produced 42 t Au, or 1.36 Moz, with only a small portion of the cumulative

production from Zone 5. Agnico Eagle Mines Limited acquired the Bousquet property in 2003 and initiated an extensive exploration program on the Zone 5 in 2010, confirming the potential of this mineralized body at depth. Following positive results, mine development started in 2017, and the LZ5 mine achieved commercial production on June 1, 2018 (Agnico Eagle Mined Limited, 2021).

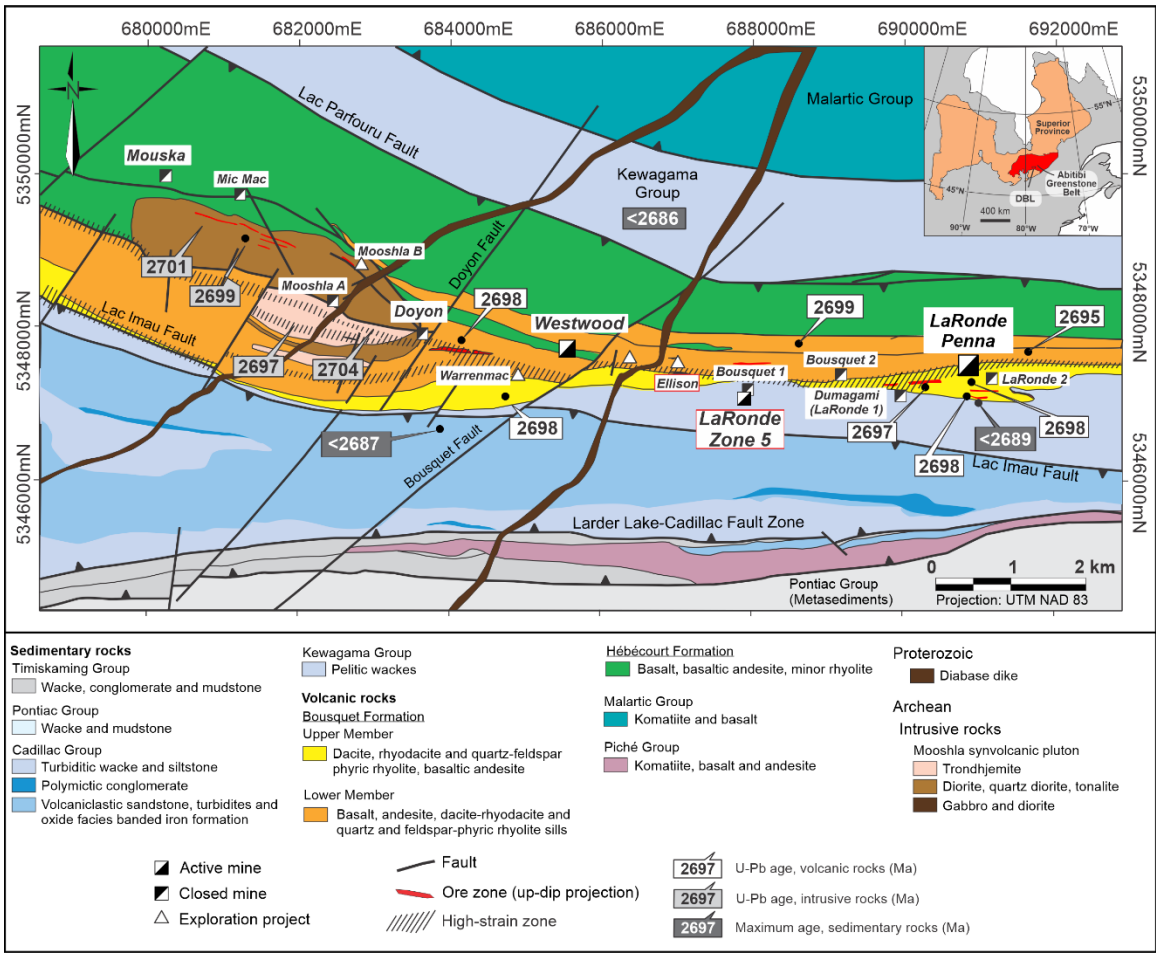

Figure 2. Simplified geology of the Doyon-Bousquet-LaRonde mining camp. From Mercier-Langevin et al. (2017).

As of the end of 2020, the LZ5 mine has produced 2.06 Mt of ore at an average head grade of 2.19 g/ Au for a total of 145,000 ounces (4.5 t) of Au. Total reserves (proven and probable) and resources (indicated and inferred) at the same date were estimated at 18.5 Mt of ore at 1.96 g/t for a total of 36.3 t Au (1.17 Moz) (Agnico Eagle Mines Limited, 2021). The Ellison mineralized corridors (Zone A and Zone B) are the westward extension to some of the LZ5 ore zones into the Ellison property, which is adjacent to the Bousquet property. Resources (indicated and inferred) for the Ellison property mineralized zones were estimated at 8.5 Mt at 2.4 g/t Au at the end of 2020 (Agnico Eagle Mines Limited, 2021).

Because LZ5 has been less studied than other deposits of the district, and because it has its own characteristics, uncertainties remain as to the exact timing of Au

mineralization, model of formation, and type of deposit. For example, the transposed networks of auriferous pyrite ±chalcopyrite-pyrrhotite-sphalerite veins and veinlets, and lesser disseminated and fragmental pyrite, strongly contrast with the semi-massive to massive sulfide and sulfide-quartz styles of mineralization more common in the DBL camp. The LZ5 mineralization is also depleted in base metals and Ag relative to the other types of mineralization in the DBL camp. The absence of a massive sulfide lens and the presence of Au and sulfide-rich discordant quartz-carbonate veins crosscutting the mineralization further complicate the classification and genesis of this deposit that has often been considered atypical.

This report presents results from the study of the alteration and ore assemblages of the LZ5 deposit and the Ellison mineralized zones. It complements results presented in Boily-Auclair et al. (2020) on the stratigraphic setting of the LZ5 and Ellison mineralized zones. This report aims to provide a better understanding of the relative timing of events, to provide a model of formation, to compare the mineralization with other styles present in the DBL camp, and to contribute to the metallogenic models for Archean Au deposits in Archean greenstone belts.

REGIONAL GEOLOGICAL SETTING

The Abitibi greenstone belt is composed of mafic to felsic volcano-sedimentary assemblages that range in age from ~2795 Ma to 2695 Ma that are cut by synvolcanic to post-tectonic intrusions (Fig. 1) (Chown et al., 1992; Ayer et al., 2002; Thurston et al., 2008; Monecke et al., 2017; Dubé and Mercier-Langevin, 2020). The Abitibi belt is bounded to the north by the Opatica Subprovince, to the southeast by the Pontiac metasedimentary Subprovince and to the south and southwest by the Paleoproterozoic rocks of the Huronian Supergroupto the east by the Mesoproterozoic Grenville tectonic zone, and to the west by the gneisses of the Kapuskasing structural zone (Fig. 1) (Robert, 1989; Sawyer and Benn, 1993; Calvert et al., 1995; Clowes et al., 1996; Perry et al., 2006; Monecke et al., 2017).

The Abitibi greenstone belt hosts numerous precious metal deposits that are commonly located along or near major east-west trending brittle-ductile deformation zones that crosscut the belt (Fig. 1). The two most fertile deformation zones in the southern part of the Abitibi are the Larder-Lake Cadillac fault zone (LLCDZ) to the south and the Destor-Porcupine fault zone (DPDZ) to the north. Both fault zones are steeply dipping (70-90°). The fault zones are long-lived structures that have controlled volcanism and sedimentation since at least 2679 Ma (Monecke et al., 2017 and references therein). A total endowment of 3,471 t Au (105.4 Moz) has been estimated for the orogenic Au deposits situated along the LLCDZ and 2,766 t Au (88.9 Moz) for the ones situated along the DPDZ (Dubé and Mercier-Langevin, 2020).

The Abitibi greenstone belt also contains ~ 775 Mt of volcanogenic massive sulfide (VMS) ore, formed during distinct episodes of submarine volcanism (Monecke et al., 2017). About 1,190 t (13%) of the Au present in the Abitibi greenstone belt comes from synvolcanic auriferous sulfide lenses and sulfide veins (Dubé and Mercier-Langevin,

2020). The various episodes of submarine volcanism are characterized by different styles of VMS deposits (Mercier-Langevin et al., 2011; Dubé and Mercier-Langevin, 2020). For example, one of the world's largest VMS, the Kidd Creek Cu-Zn deposit, is hosted within a succession of mafic-ultramafic and felsic volcanic rocks of the 2719-2711 Ma Kidd-Munro assemblage (Bleeker, 1999; Monecke et al., 2017). In contrast, the world-class LaRonde Penna Au-rich VMS deposit is hosted within felsic volcanic rocks of the 2704-2695 Ma Blake River Group (Mercier-Langevin et al., 2007a). Approximately 46% of the total VMS tonnage of the Abitibi belt and 90% of the synvolcanic Au is hosted in the deposits of the Blake River Group, indicating a favourable synvolcanic Au heritage that has no equivalent in the other Archean volcanic assemblages of the Abitibi belt (Mercier-Langevin et al., 2011, 2014; Dubé and Mercier-Langevin, 2020).

Areas outside of the LLCDZ, DPDZ, and established VMS camps, also have potential for Au, as shown by the reopening of the ~25 Moz world-class Detour Lake gold deposits in 2013, the discovery of the Bug Lake/Martiniere deposit by Balmoral Resources Ltd., the discovery of the Tabasco and Area 51 mineralized zones by Wallbridge Mining on the Fenelon Gold property in 2018, and the renewed exploration of the ~5 Moz Au Windfall deposit east of Lebel-sur-Quévillon (Fig. 1) (Kirkland Lake Gold Limited, 2020; Osisko Mining Inc., 2020; Wallbridge Mining Company Limited., 2020). This shows that there is still much potential in the belt, with a wide variety of styles and ages of Au mineralization (e.g., Dubé and Mercier-Langevin, 2020).

DOYON-BOUSQUET-LARONDE MINING CAMP

The Doyon-Bousquet-LaRonde mining camp is located in the southern part of the Abitibi greenstone belt, 2 km north of the LLCDZ, halfway between the cities of Rouyn-Noranda and Val-d'Or (Fig. 1). It is of primary economic importance in Canada with a total estimated endowment of 894 t Au (28.7 Moz; past production, estimated, proven, and probable reserves, and measured, indicated, and inferred resources: Mercier-Langevin et al., 2017). Many deposits have been, or are currently exploited, within this prolific mining camp: Doyon, Mouska, Mic Mac, Mooshla B, Bousquet 1, Bousquet 2-Dumagami, LaRonde Penna, Westwood, and LaRonde Zone 5 (Mercier-Langevin et al., 2021).

The DBL mining camp is located in the eastern part of the 2704–2695 Ma Blake River Group. The oldest volcanic formation in the study area is the Hébécourt Formation, which consists of tholeiitic basalt and basaltic andesite flows with thin gabbroic sills and local rhyolite and rhyodacitic flows. The overlying Bousquet Formation contains various proportions of basaltic to rhyolitic flows, domes, and synvolcanic intrusions (Figs. 2, 3) (Lafrance et al., 2003, 2005). The Bousquet Formation contains two informal members, lower and upper, and is dominated by tholeiitic units at its base, and by calc-alkaline units in its upper part (Lafrance et al., 2003; Mercier-Langevin et al., 2007a). Both formations are bounded to the north and the south by sedimentary rocks of the $\leq$2684 $\pm$1 Ma Kewagama Group and by the $\leq$2687 $\pm$3 Ma Cadillac Group, respectively (Figs. 2, 3) (Davis, 2002). The volcanic rocks of the Hébécourt and Bousquet formations are cut by the synvolcanic (2698-2697 Ma) Mooshla intrusion (Galley and Lafrance, 2014; McNicoll et al., 2014). The Mooshla intrusive body or its parent magmatic chamber may have played

an essential role in the formation of sulfide-quartz auriferous vein systems (Doyon deposit and Westwood deposit Zone 2 Extension) and VMS deposits of the camp by providing heat, hydrothermal fluids, and metals (Dubé et al., 2007, 2014; Mercier-Langevin et al., 2007d; Galley and Lafrance, 2014; Yergeau, 2015; Yergeau et al., 2022a, b).

The rocks of the DBL mining camp have undergone three main episodes of deformation. Hubert et al. (1984) recognized, on a local scale, an initial phase of oblique convergence (D_1) , followed by a north-south compression phase (D_2), represented by a well-developed foliation (S_2) throughout the DBL mining camp. The steeply south-dipping (~75 to 90°) east-west regional foliation (regional S_3 in Dubé and Mercier-Langevin, 2020) affects most of the rocks and mineralized lenses in the DBL camp. The last deformation episode (local D_3) is much less significant than the first two and is not as apparent in the rocks of the Blake River Group. However, it is represented by a northeast-southwestern (local S_3) cleavage that corresponds to a late deformation episode unrelated to the first two episodes (Hubert et al., 1984; Mercier-Langevin et al., 2007a; Yergeau, 2015; Yergeau et al., 2022a).

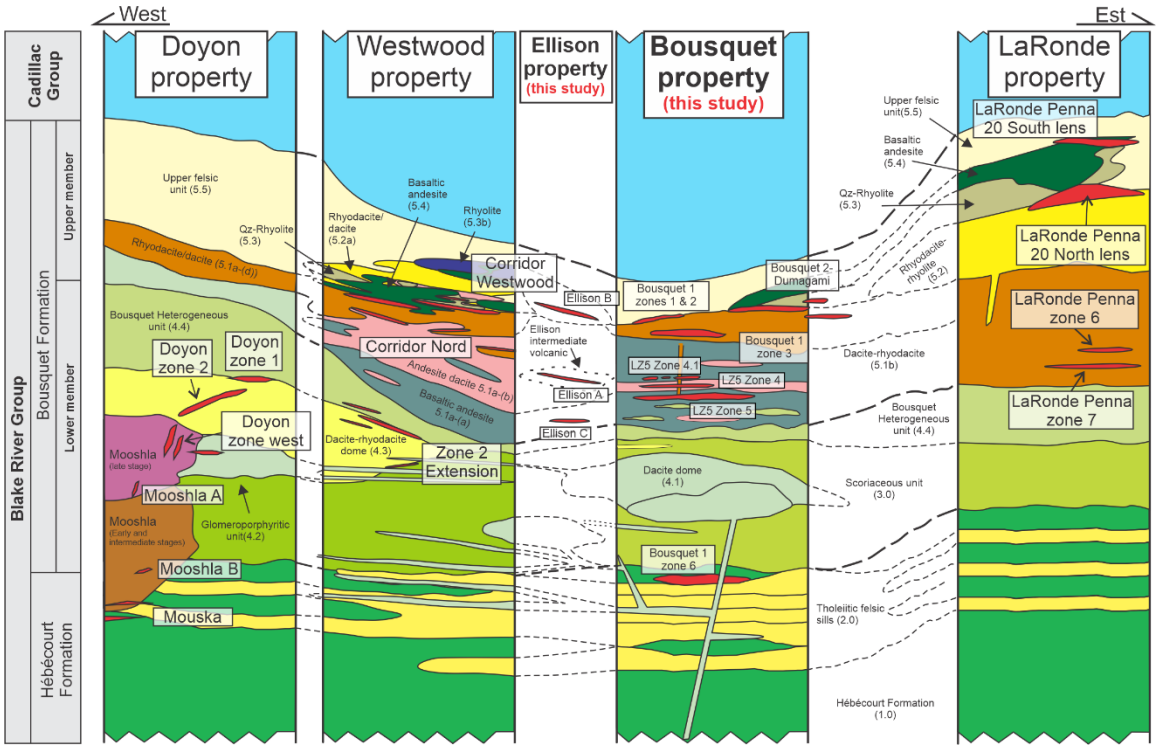

Figure 3. Simplified stratigraphic columns of the Doyon-Bousquet-LaRonde mining camp showing the stratigraphic position of the main mineralized zones of the Doyon, Westwood, Ellison, Bousquet, and LaRonde properties. The ore lenses are not to scale. Modified from Lafrance et al. (2003), Mercier-Langevin (2005) and Yergeau (2015).

The mineralized zones of the LZ5 deposit and Ellison property are hosted within a succession of volcanic and volcaniclastic mafic to felsic units of the Bousquet Formation upper member (Boily-Auclair et al., 2020). The rocks are strongly altered, deformed, and metamorphosed to greenschist facies. Three distinct mineralized corridors compose the LZ5: Zone 4.1, Zone 4, and Zone 5. Zone 5 is the main mineralized body, whereas zones

4 and 4.1 are thin discontinuous mineralized corridors that only account for a small proportion of the LZ5 total Au budget (Figs. 4, 5). The mineralized zones on the Ellison property are located a few hundred meters west of the LZ5 and define three stacked corridors: zones A, B, and C (Fig. 3).

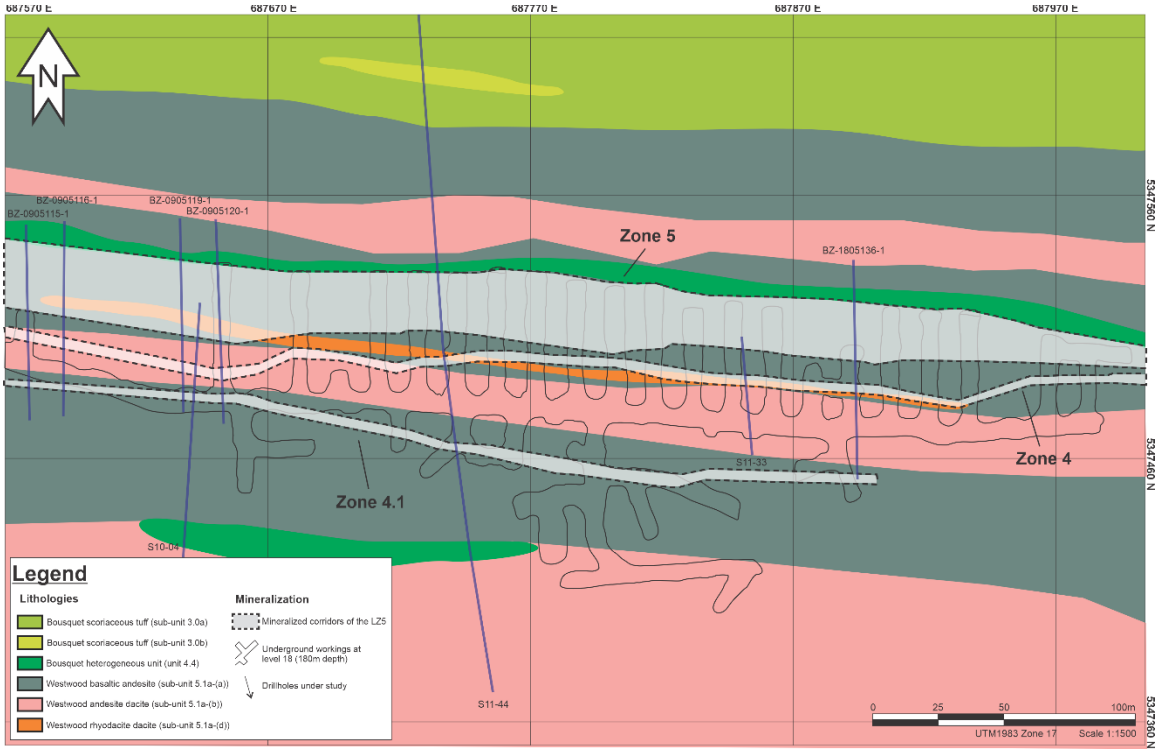

Figure 4. Simplified geological map (plan view) of level 18 (180 m below surface) showing the distribution of the units hosting the mineralized corridors of zones 4, 4.1, and 5 of the LZ5 mine (Agnico Eagle Mines Ltd, 2019). This figure was made from several boreholes that have different dips. This is a composite drawing and projection problems may affect the geological interpretation.

SUMMARY OF THE LARONDE ZONE 5 AND ELLISON PROPERTY HOST ROCKS

The LZ5 and the mineralized zones of the Ellison property were, until recently, interpreted as being hosted in the uppermost part of the Bousquet Formation lower member, i.e., in the Bousquet heterogeneous unit (unit 4.4: Lafrance et al., 2003; Mercier-Langevin et al., 2007d). Careful underground mapping, drill core logging, and whole-rock geochemistry allowed Boily-Auclair et al. (2020) to show that the ore zones are instead hosted in the lowermost part of the highly fertile Bousquet Formation upper member, i.e. slightly higher in the stratigraphy than previously thought (Fig. 3). Although this remains true, further work allowed for minor updates to the classification of some samples and a slight revision of the stratigraphic setting of the LZ5 and Ellison mineralized zones. Therefore, the summary presented here presents a slightly revised version of the geology of the study area relative to what has been published in Boily-Auclair et al. (2020). Among the most significant changes is the definition of a newly described unit on the Ellison property previously considered part of the Westwood basaltic andesite (subunit 5.1a-(a)) now referred to as the Ellison intermediate volcanic unit.

The LZ5 is hosted in the Westwood andesitic to rhyodacitic unit (unit 5.1a), which forms the base of the upper member of the Bousquet Formation in the central part of the DBL camp (Yergeau et al., 2022a). The Ellison Zone A is hosted within a volcanic unit of intermediate composition that has not been documented elsewhere in the DBL camp. This unit has a geochemical signature similar to that of the Bousquet heterogeneous unit (unit 4.4) but is however located higher in the stratigraphic sequence. Because of that, it has previously been considered a potentially more mafic part of the Westwood andesitic to rhyodacitic unit (unit 5.1a) (Boily-Auclair et al., 2020). The Ellison Zone B mineralized corridor is hosted in the Westwood feldspar-phyric rhyolitic dome (subunit 5.3a-(b)). The Bousquet heterogeneous unit (unit 4.4), which is up to 300 m thick on the Westwood property, east of the LZ5 deposit, is present only as thin, discontinuous bands intercalated within the Westwood basaltic andesite (subunit 5.1a-(a)) and the Westwood andesite-dacite (subunit 5.1a-(b)) on the Bousquet property (Fig. 4).

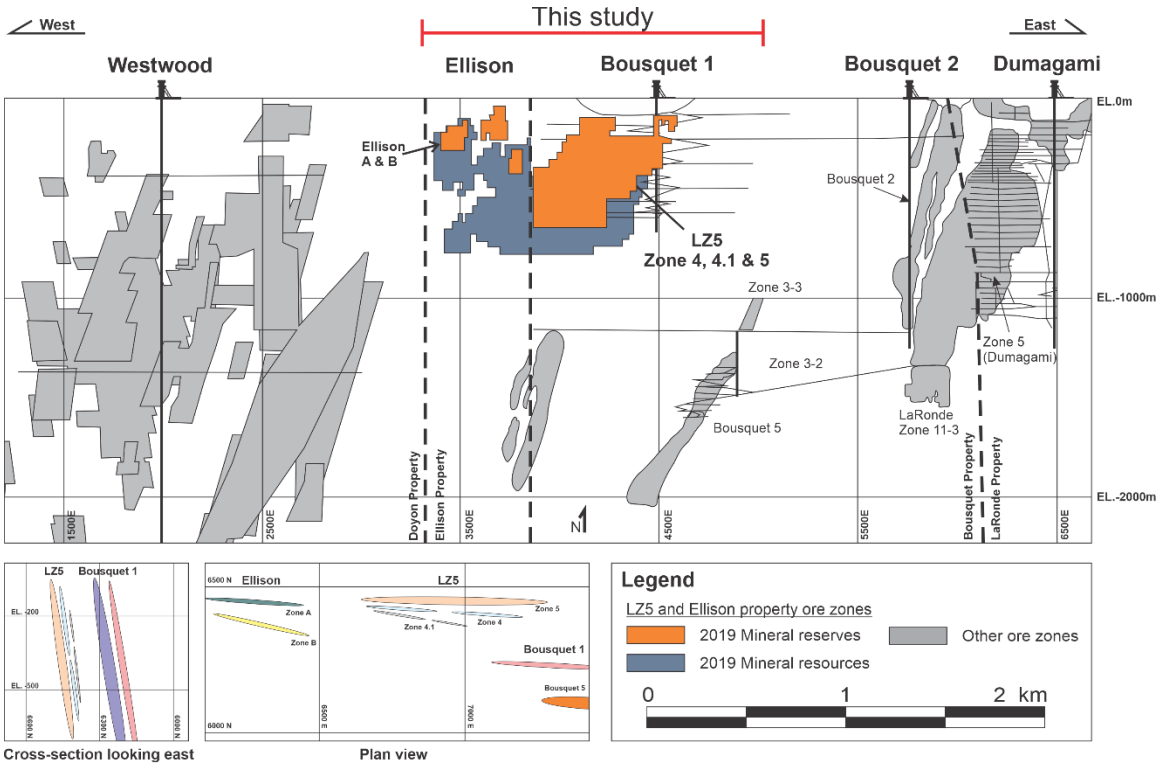

Figure 5. Composite longitudinal section (looking north) of the Westwood, Ellison, and Bousquet properties showing the distribution of the main mineralized zones of the Westwood, Ellison, LZ5, Bousquet 1, and Bousquet 2-Dumagami deposits. Modified from Mercier-Langevin et al. (2009). Data from Agnico Eagle Mines Limited (2021).

Footwall Units of the LaRonde Zone 5 and Mineralized Zones of the Ellison Property

The base of the Bousquet Formation lower member on the Bousquet property consists of tholeiitic to calc-alkaline, mafic to felsic volcanic and volcaniclastic units, and sills or dykes (Fig. 3). The tholeiitic to transitional sub-alkaline basalts and transitional andesites of the Bousquet scoriaceous tuff (unit 3.0) are intercalated with thin (<10 m) and massive

intermediate to felsic sills or dykes of transitional to calc-alkaline magmatic affinity of the Bousquet dacitic dome (unit 4.1), lobe hyaloclastite-type flows of the Doyon glomeroporphyritic unit (unit 4.2) and sills or dykes of the Doyon felsic unit (unit 4.3) (Fig. 3). The Bousquet scoriaceous tuff is divided into two subunits based solely on their geochemical characteristics: subunit 3.0a and subunit 3.0b. Subunit 3.0a is of mafic composition, whereas subunit 3.0b has a more intermediate composition (Fig. 6a, b). Unit 3.0, therefore, consists of complex intercalation of lapilli tuff and/or tuff breccia, lava flows, flow breccias, and rare fine tuffs of mafic to intermediate composition that makes up most of the footwall of the LZ5 ore zones. In the former Bousquet mine area, rocks of unit 3.0 are strongly altered to chlorite, biotite, and carbonates in addition to being very intensely deformed, making the identification of volcanic facies very difficult (Yergeau, 2015; Boily-Auclair et al., 2020).

As stated earlier, thin bands (up to 15 m thick) of the Bousquet heterogeneous unit (unit 4.4) are present in the immediate footwall and hanging wall, of the LZ5 deposit. They are intercalated within the Westwood basaltic andesite (subunit 5.1a-(a)) and Westwood andesite-dacite (subunit 5.1a-(b)). This intercalation suggests that the magmatism of the Bousquet Formation lower member was still active when the volcanism of the upper member started. However, this may also be due to, or it may have been accentuated by, tectonic transposition during regional deformation.

Host and Hanging-Wall Units of the LaRonde Zone 5 and Mineralized Zones of the Ellison Property

The LZ5 zones 4.1, 4, and 5 are hosted in massive to fragmental intermediate rocks of the Westwood andesitic to rhyodacitic unit (unit 5.1a). The Westwood andesitic to rhyodacitic unit has been divided into four subunits by Yergeau et al. (2015) based on texture and composition: the Westwood basaltic andesite (subunit 5.1a-(a)), the Westwood andesite-dacite (subunit 5.1a-(b)), the Westwood mafic sills (subunit 5.1a-(c)), and the Westwood dacite-rhyodacite (subunit 5.1a-(d)). The names of these subunits were slightly modified in Yergeau et al. (2022a, b). The first two compose most of the LZ5 deposit host rocks, hanging wall, and immediate footwall (Boily-Auclair et al., 2020) (Fig. 6a, b, c). The Westwood basaltic andesite mainly consists of aphanitic to finely grained volcanic rocks and/or mafic sills with a minor monogenic lapilli tuff and tuff breccia component with rounded to angular fragments. When very fresh, this subunit contains 5 to 15 vol. % mm-sized feldspar phenocrysts. The Westwood basaltic andesite is also characterized by the presence of quartz-carbonate and mm- to cm-size amygdales (Yergeau, 2015; Boily-Auclair et al., 2020; Yergeau et al., 2022a, b). The Westwood andesite-dacite is largely composed of massive volcanic rocks of intermediate to felsic composition with a minor volcaniclastic component including lapilli tuffs and tuff breccias (Fig. 6a, b). Yergeau (2015) interpreted the volcaniclastic rocks as talus breccia deposits as they are polymictic, contain angular clasts, are laterally limited, and locally contain lithic and massive sulfide fragments.

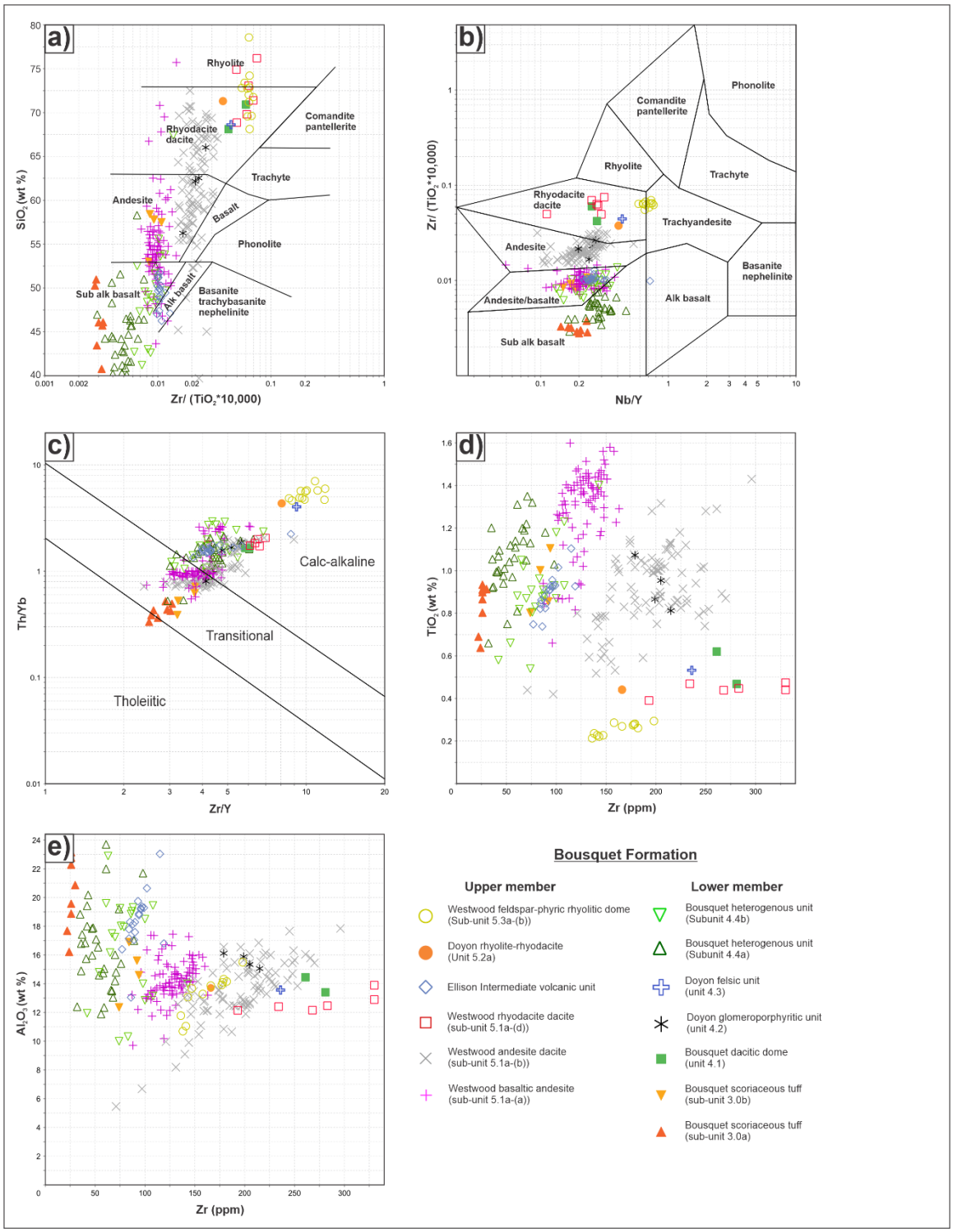

Figure 6. Major and trace element plots for the volcanic, volcaniclastic, and intrusive rocks of the Bousquet Formation upper and lower member from the LZ5 and Ellison areas, sampled in drillholes S10-04, S11-33, S11-44, BZ-0905115-1, BZ-0905116-1, BZ-0905119-1, BZ-0905120-1, BZ-1805136-1, 121-06-11, 121-06-16, and 121-06-20 (*see* Fig. 4 for the location of drillholes). **a)** and **b)** Winchester and Floyd (1977) volcanic rock classification diagrams. **c)** Ross and Bédard (2009) magmatic affinity diagram. **d)** TiO_2 versus Zr. **e)** Al_2O_3 versus Zr.

A felsic sill or dyke cuts the LZ5 mineralized zones. This thin intrusive body is strongly altered, deformed, and mineralized (up to 20 vol. % Py) and crosscuts the Doyon dacite-rhyodacite unit. It can be followed from the eastern part of the LZ5 mineralized corridor to the Ellison property to the west. The nature of this intrusive body is not clear as the intense alteration and deformation of this unit make it almost impossible to properly characterize the protolith. This unit has been geochemically associated with the Upper felsic unit (unit 5.5) in 2020 due to its low Ti content, high Zr content, and very high SiO_2 content (Fig. 6a, b, d) (Boily-Auclair et al., 2020). However, it's stratigraphic position (i.e. at the base of the Bousquet Formation upper member) indicates that this intensely altered felsic unit could instead be geochemically correlated with the Westwood dacite-rhyodacite. More work would be needed to properly characterize this unit.

The Ellison Zone A is hosted within calc-alkaline intermediate volcanic rocks that are geochemically similar to the Bousquet heterogeneous unit (unit 4.4) (Fig. 6a, b, c). However, this newly described unit ("Ellison intermediate volcanic unit", Fig. 6) is located much higher in the stratigraphic sequence than elsewhere in the DBL camp, at the contact with the Westwood feldspar-phyric rhyolitic dome (subunit 5.3a-(b)). The Ellison Zone A host rocks consist of massive and coherent volcanic rocks of basaltic andesite composition. The host unit also contains up to 3 vol. % fine quartz-carbonate amygdales (5–10 mm in size). The limited amount of material from the Ellison ore zones collected in this study makes it difficult to adequately define this unit. More work would be needed on the Ellison property to better describe the host unit of the Ellison Zone A. The Ellison intermediate volcanic unit also shows a high Al_2O_3 content and low TiO_2 and Zr contents, similar to the Bousquet heterogenous unit signature (Fig. 6d, e).

The Ellison Zone B is hosted in the Westwood feldspar-phyric rhyolitic dome (subunit 5.3a-(b)) that is predominantly composed of lapilli tuffs and tuff breccias, with, more rarely, thin bands of massive feldspar-rich volcanic rocks. The fragments in the volcaniclastic rocks are monogenic, of felsic composition with a siliceous appearance, and make up 50 to 80 vol. % of the rock (Fig. 6a, b) (Yergeau, 2015; Boily-Auclair et al., 2020).

MINERALIZATION STYLES OF THE LARONDE ZONE 5 AND ELLISON ORE ZONES

Mineralized zones at LZ5 and at the Ellison property consist of stratigraphically stacked Au-rich corridors that are variably continuous laterally and at depth (Figs. 4, 5; Table 1). The LZ5 orebody comprises three distinct mineralized corridors that are, from south to north: Zone 4.1, Zone 4, and Zone 5. The latter is the main mineralized body, whereas zones 4 and 4.1 are considered as satellite, discontinuous, ore zones (Fig. 4). The Ellison property mineralized zones are located a few hundred meters west of the LZ5 deposit and consist of three stacked mineralized corridors (Zone A, Zone B, and Zone C) (Fig. 3). Zone A is hosted within an intermediate volcanic unit, at a very similar stratigraphic position to the LZ5 ore zones. Zone B is located higher in the stratigraphic sequence, within the Westwood feldspar-phyric rhyolitic dome (subunit 5.3a-(b): Boily-Auclair et al., 2020). The Ellison Zone C has not been intercepted in any of the studied drill holes and will therefore not be discussed here.

LaRonde Zone 5 Mineralized Corridors

The LZ5 mineralized corridors are subvertical (~80°) and parallel with the main E-W foliation (S_2). The corridors generally dip steeply to the south and plunge to the south-west. The mineralized zones are metamorphosed, flattened by D_2, transposed, and parallel to sub-parallel with the main foliation. The main mineralized zone (Zone 5) has a width of 600 m (E-W), a vertical extent of more than 1 km, and a maximum thickness (N-S) of 30 m (Figs. 4, 5). Although Zone 5 can be traced from east to west over approximately 850 m, the main mineralized body thins at both ends to a couple of meters wide or less where it becomes sub-economic because of a lack of volume (Figs. 4, 5). In detail, Zone 5 consists of a broad mineralized envelope that contains two enriched corridors separated by a slightly lower grade core (~2 to 3 g/t Au for the south and north parts versus ~1 g/t Au for the central part). The lower grade core becomes thicker at depth with a gradual decrease in the average Au grade (Fig. 7).

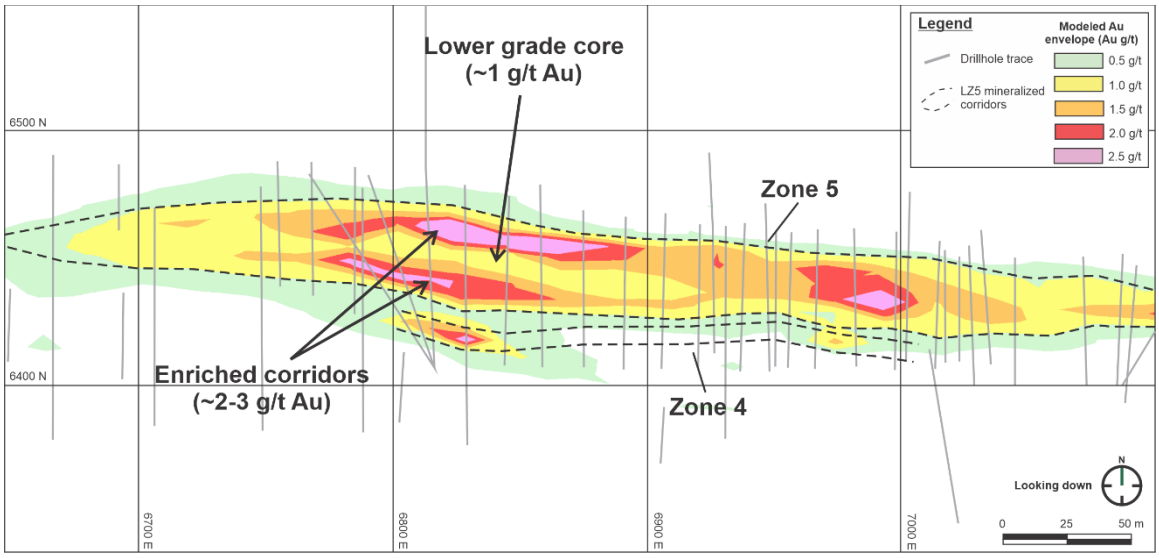

Figure 7. Plan view of level 300 (300 meters below the surface) showing the modeled enriched corridors (~2–3 g/t Au) and lower grade core (~1 g/t Au) of the Zone 5 of the LZ5 mine. The numerical model was made using Seequent's LeapFrog Geo modeling software and the Agnico Eagles Mines Ltd. geochemical Au assays database. The radial distance function was used to generate this model with a N180°/80° structural trend to take into account the main D2 deformation event that affects ore and alteration.

The principal style of mineralization is characterized by a stockwork of mm- to cm-thick veins and veinlets (10–20 vol. %) (Fig. 8a). These are strongly flattened and partly transposed into the main E-W, steeply south-dipping S_2 foliation (Fig. 8b). Finely disseminated sulfides and/or elongated/flattened cm- to dm-long sulfide clasts that most likely represent boudinaged veins (≤5 vol. %) are also present but do not represent the principal Au mineralization of Zone 5. The veins, veinlets, and disseminations are almost exclusively composed of pyrite, with trace amounts of pyrrhotite, chalcopyrite, and sphalerite. Centimeter-wide sphalerite-pyrite veins that are sub-concordant with the stratigraphy are also common within the mineralized zones of the LZ5 deposit (Fig. 8c). Gold is present as inclusions within the granoblastic pyrite and commonly occurs in the

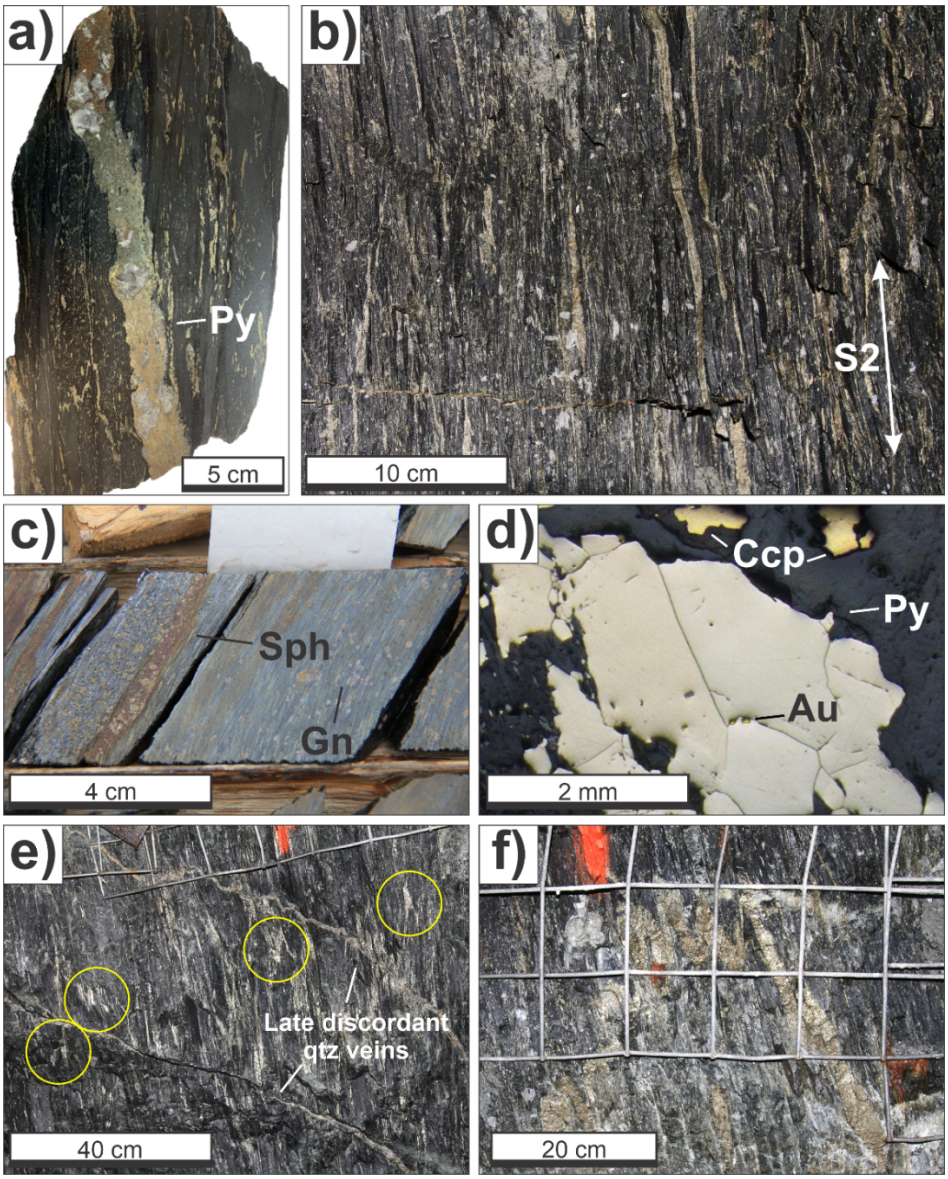

Figure 8. a) Polished slab of a 2-3 cm-thick pyrite-quartz vein with thinner pyrite veinlets typical of the Zone 5 of the LZ5 mine. Note that the vein and veinlets are sub-parallel to, or transposed into, the S_2 foliation and are locally folded and boudinaged. Photograph by E. Boily-Auclair, NRCan photo 2021-678. **b)** 12-15% mm-thick stringers of pyrite that are sub-concordant with the stratigraphy in a massive and homogeneous basaltic-andesitic rock (subunit 5.1a-(a)). Note the strong S_2 foliation developed in the host rock. Development gallery PS-12-05-118, level 12. Photograph by P. Mercier-Langevin, NRCan photo 2021-679. **c)** Millimetre-thick sphalerite-pyrite vein with garnet porphyroblasts in a sericite and chlorite-altered dacitic-andesitic rock (subunit 5.1a-(b)) in Zone 4. The sphalerite vein is parallel with the S_2 foliation. Drillhole S11-44. Photograph by P. Mercier-Langevin, NRCan photo 2021-680. **d)** Photomicrograph (reflected polarized light) of granoblastic pyrite. Gold is present as inclusions at and near the triple junctions of the recrystallized pyrite. Drillhole BZ-1805136-1. Photograph by E. Boily-Auclair, NRCan photo 2021-681. **e)** Mineralized corridor of Zone 5 (pyrite veins and veinlets) in a massive basaltic-andesitic host-rock (subunit 5.1a-(a)). The veins are intensely folded and transposed into the S_2 foliation. The circled hinges represent a single vein that has been dismembered into the foliation. Note the presence of two late discordant millimetric quartz veins at high angle to the pyrite veinlets and foliation. Development gallery PS-18-05-134, level 18. Photograph by P. Mercier-Langevin, NRCan photo 2021-682. **f)** Pyrite-rich veinlet folded by D_2 in Zone 5. Development gallery PS-12-05-118, level 12. Photograph by P. Mercier-Langevin, NRCan photo 2021-683.

triple junctions of the recrystallized pyrite (Tourigny et al., 1989a; Boily-Auclair et al., 2019; Fig. 8d). Most of the veins are strongly transposed and folded into the S_2 foliation (Fig. 8e, f). Clasts or boudins of veins and veinlets that were intensely foliated and flattened in S_2 are also present. Very small, elongated ilmenite grains (>0.1 mm) are present in or near the ore zones. The grains are disseminated through the matrix and are oriented into S_2 (Boily-Auclair, 2017).

Discordant cm- to dm-thick quartz-carbonate veins, locally rich in pyrite and chalcopyrite (up to 20–30 vol. %), locally cut across the LZ5 mineralized zones (Fig. 9a). No significant or particular alteration is present in the periphery of the veins. Grades of up to 60 g/t Au over 1.5 m are occasionally associated with these veins (Boily-Auclair et al., 2019). When these quartz veins intersect mineralized zones that are rich in auriferous sulfides, the latter are often partially remobilized in the quartz veins (Fig. 9b). Outside of the mineralized zones and their sulfide-rich envelope, the quartz-carbonate veins are barren, suggesting that Au in these quartz-carbonate veins is due to local remobilization of the metals.

Ellison Property Mineralized Zones

Zones A and B at Ellison are located west of the LZ5 deposit (Fig. 5). The zones consist of narrow mineralized corridors (≤3 m thick) of sulfide veins, stockworks, disseminations, and narrow semi-massive to massive sulfide bands. The mineralized zones extend laterally over about 400 m and extend from the surface to a depth of approximately 400 m. Mineralized intervals have been intercepted at greater depth (up to 4 g/t Au over 5.5 m at 1,100 m vertical depth). The Ellison Zone A has an east-west orientation, similar to the Zone 4 and Zone 5 of the LZ5, whereas the Ellison Zone B has a north-west to south-east orientation, similar to zones 1 and 2 at the former Bousquet 1 mine (Fig. 5).

The auriferous mineralization in Zone A consists of concentric bands of disseminated sulfide (5–25 vol. %) with local sulfide veinlets and dm-wide recrystallized semi-massive sulfide-rich bands (50–75 vol. %). The veinlets are strongly transposed into the foliation. Pyrite is the main mineral phase and is finely to coarsely recrystallized (0.1–10 mm) (granoblastic) within diffuse or concentrated bands transposed into the foliation (Fig. 9c) (Lair, 2007). Locally, up to 10 vol. % of sphalerite and chalcopyrite are present within the mineralized bands (Mercier-Langevin, 2006). Chalcopyrite is less abundant, forming up to 5 vol. % of the rock over short intervals (less than 50 cm), and is generally interstitial to pyrite in transposed semi-massive to massive bands and in a few isolated thin veinlets (Mercier-Langevin, 2006). Sphalerite, although more abundant than chalcopyrite, is much less abundant than pyrite, exceptionally forming up to 10 vol. % of the constituents over short intervals (≤20 cm). Sphalerite forms thin transposed bands or forms an interstitial phase in transposed bands of semi-massive to massive pyrite and in a few isolated thin veinlets of pyrite-sphalerite (Mercier-Langevin, 2006). Sphalerite and chalcopyrite are not necessarily associated with higher Au grades. Pyrrhotite is also present in trace amounts and associated with pyrite (up to 1 vol. % locally). Lead-rich and Bi-rich telluride inclusions in the granoblastic pyrite are present in Zone A (Lair, 2007).

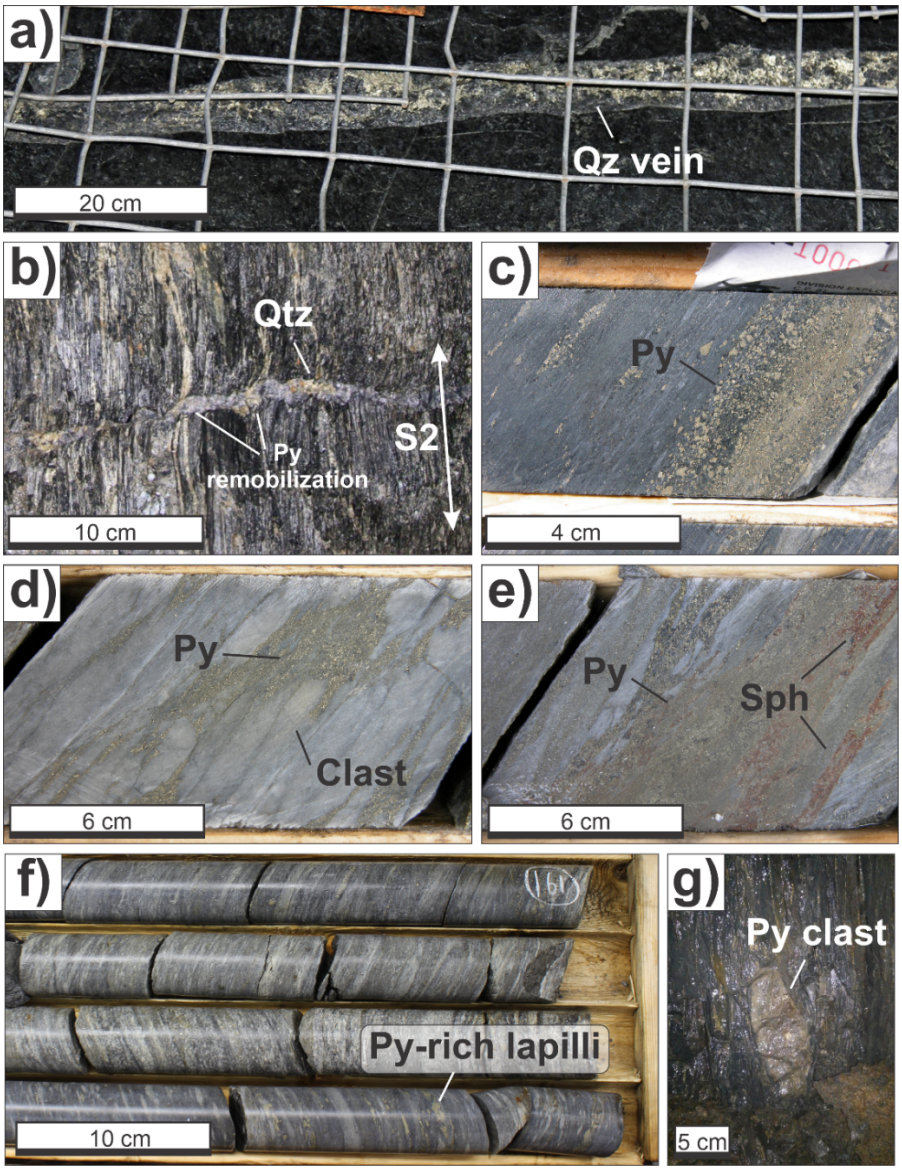

Figure 9. a) Late, discordant sub-horizontal Au and sulfide-rich quartz-carbonate vein. Showing the south wall of a longitudinal gallery, the photograph is taken looking south, looking at the foliation plane. Development gallery PS-12-05-112, level 12. Photograph by P. Mercier-Langevin, NRCan photo 2021-684. **b)** Discordant quartz-carbonate vein crosscutting the mineralized corridor of Zone 4. Note the remobilization of sulfides along the quartz-carbonate vein. Development gallery PS-18-05-134, level 18. Photograph by E. Boily-Auclair, NRCan photo 2021-685. **c)** Typical diffuse band of finely disseminated granoblastic pyrite (0.1 to 1 mm) in an intermediate volcanic unit typical of the Ellison Zone A. Drillhole 121-06-11. Photograph by P. Mercier-Langevin, NRCan photo 2021-686. **d)** Typical mineralization observed within the Ellison Zone B. Pyrite-rich vein and veinlets transposed and concentrated around the clasts in a felsic volcaniclastic host unit (5.3a-(b)). Drillhole 121-06-20. Photograph by P. Mercier-Langevin, NRCan photo 2021-687. **e)** Transposed sphalerite veinlet in a semi-massive pyrite-rich band in the Ellison Zone B. The mineralization is hosted within a felsic volcaniclastic unit (5.3a-(b)). Drillhole 121-06-20. Photograph by P. Mercier-Langevin, NRCan photo 2021-688. **f)** Pyrite-rich mafic lapilli tuff present in the footwall of Zone 5 in a basaltic andesite volcaniclastic host unit (5.1a-(a)). Drillhole BZ-1805136-1. Photograph by E. Boily-Auclair, NRCan photo 2021-689. **g)** Massive pyrite clast in the immediate footwall of Zone 5 in a massive dacite-andesite host-unit (5.1a-(b)). Development gallery PS-09-05-127, level 9. Photograph by M. Bernier, NRCan photo 2021-690.

Zone B consists of a discordant network of mm- to cm-thick pyrite ±chalcopyrite ±sphalerite veins and veinlets (10–20 vol. %), disseminated pyrite, and thin local semi-massive pyrite bands. The veinlets are transposed into the S_2 foliation and are concentrated around the clasts in the fragmental felsic volcanic host unit (Fig. 9d) (Mercier-Langevin, 2006). The pyrite is finely recrystallized (0.1–1 mm). Bands of semi-massive pyrite are present very locally (25–50 vol. %; up to 10 cm thick: Nadim, 2007). Variable, but overall minor amounts, of chalcopyrite, sphalerite, and pyrrhotite are present within the mineralized corridor. Remobilized chalcopyrite veinlets are locally present. Sphalerite is found within the semi-massive pyrite bands as strongly transposed veinlets (Fig. 9e) (Mercier-Langevin, 2006). Significantly higher Au grades are generally associated with elevated Cu and Zn grades (e.g., 25.3 g/t Au with 4.4% Cu and 3.1 % Zn over 0.2 m). Nadim (2007) also documented trace amounts of titanite, monazite, galena, Ag tellurides, and electrum in inclusions or at the triple junction of the granoblastic pyrite.

Mineralized intervals in the Ellison Zone A and Zone B are in general slightly richer but narrower than typical mineralized intervals in the LZ5 main mineralized zone (3.8 g/t Au over 1 m long intervals on average for Ellison Zone A and 1.8 g/t Au over 1 m long intervals on average for Ellison Zone B, compared to 1.5 g/t Au over 1 m long intervals on average for Zone 5 of the LZ5). Visible Au is present in Zone A in late greyish quartz veins in association with remobilized sulfides (pyrite, chalcopyrite, and sphalerite) (Mercier-Langevin, 2006). The mineralized intervals at the Ellison Zone A have an average thickness of 4.5 m, whereas the Ellison Zone B has thicker intervals on average. Silver grades are also commonly higher in Zone A with an average Au to Ag ratio of 1:1, whereas it is of 1:4 in Zone B. The Au to Ag ratio is approximately 2:1 at LZ5 based on unpublished 2020 mill results, in agreement with limited whole-rock data.

ALTERATION ASSEMBLAGES

Sericite (fine-grained muscovite), chlorite, carbonates, and local biotite are common alteration minerals in all studied mineralized corridors. However, some differences in terms of mineralogy and relative abundance of the main alteration minerals are present within the alteration halos. As rocks of mafic to felsic composition host the mineralization within the base of the Bousquet Formation upper member, the mineralogy of the associated alteration varies depending on the primary composition of the altered rocks. Rocks of the Bousquet Formation were metamorphosed to upper greenschist to lower amphibolite facies, which also impacts the current mineralogy and the alteration zones associated with the mineralized corridors. Underground mapping, drill core description, petrography and lithogeochemistry were used in conjunction to better define the alteration mineral assemblages of the LZ5 and Ellison ore zones.

Metamorphosed Hydrothermal Alteration Assemblages at LZ5

The LZ5 deposit host rocks consist mostly of volcanic and volcaniclastic basaltic andesite (subunit 5.1a-(a)) and andesite-dacite (subunit 5.1a-(b)). The alteration assemblages present in the LZ5 mine area can be divided into three main sub-groups: (1) a distal sericite-carbonate-chlorite-quartz-feldspar ±biotite assemblage; (2) an intense proximal sericite-

carbonate-chlorite-pyrite-quartz-feldspar-biotite ±epidote assemblage; and (3) a local proximal sericite-pyrite-quartz assemblage (Fig. 10, Table 1).

Distal alteration assemblages

The distal footprint of the LZ5 can be traced several tens of meters on both the footwall and hangingwall sides of the main mineralized body (Zone 5). This banded sericite-carbonate-chlorite-quartz-feldspar assemblage is mainly developed in the Westwood basaltic-andesite (subunit 5.1a-(a)) and andesite-dacite (subunit 5.1a-(b)). It is characterized by compositional bands rich in sericite-feldspar and bands rich in quartz-carbonate (Fig. 11a). The feldspars consist of syndeformation porphyroblasts elongated parallel to the main foliation (S_2) that are locally replaced by chlorite and biotite (Fig. 11b). The quartz-carbonate bands are composed of fine granoblastic quartz with coarser, sometimes elongated, carbonate grains in variable proportion (5–15 vol. %). Local very fine interstitial chlorite is present (≤5 vol. %). The compositional banding is parallel to the S_2 foliation and is possibly the result, at least in part, of mineral segregation of tectometamorphic origin (Yergeau, 2015). This distal alteration gradually intensifies closer to the mineralized zones and, more specifically, materializes as an increase in the amount of disseminated pyrite.

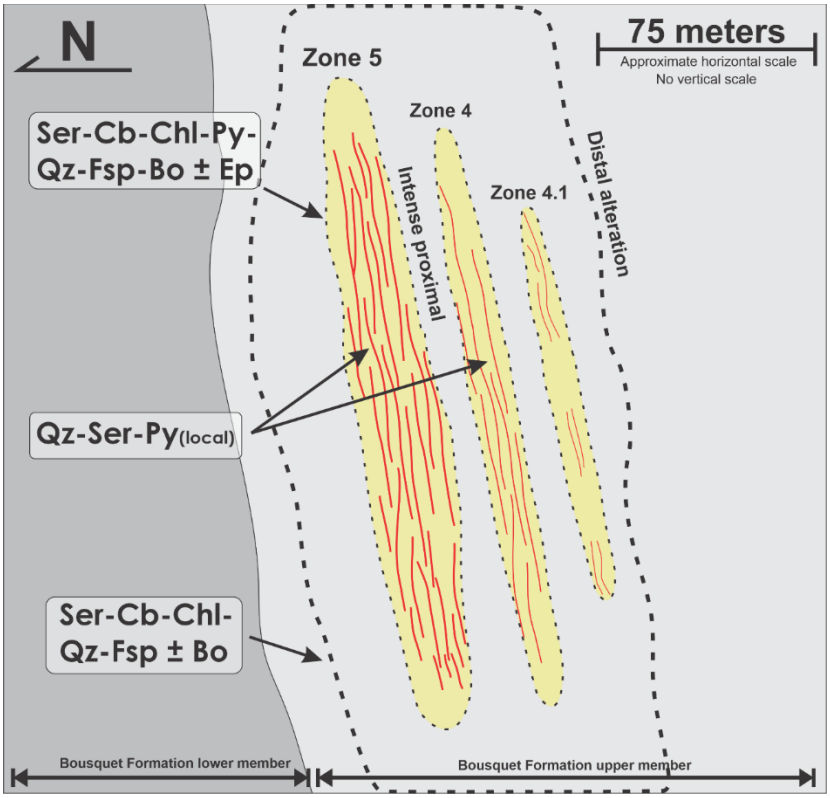

Figure 10. Simplified schematic cross-section (looking East) of the alteration assemblages present in the LZ5 mineralized corridors. The alteration assemblages can be divided into three main sub-groups: (1) a distal sericite-carbonate-chlorite-quartz-feldspar ±biotite assemblage; (2) an intense proximal sericite-carbonate-chlorite-pyrite-quartz-feldspar-biotite ±epidote assemblage; and (3) a local proximal sericite-pyrite-quartz assemblage.

Intense proximal alteration assemblages

Approximately 5 m on both hanging wall and footwall sides of the ore zones, the alteration intensifies and becomes a sericite-carbonate-chlorite-pyrite-quartz-feldspar-biotite ±epidote assemblage developed in the Westwood basaltic-andesite and the Westwood andesite-dacite (subunits 5.1a-(a) and 5.1a-(b), respectively). This alteration is characterized by mineral segregation composed of mm-wide sericite-dominated bands intercalated with mm-wide chlorite and biotite-dominated bands (Fig. 11c). Sericite comprises at least 30 vol. % of the sericite-feldspar rich bands and fine-grained epidote porphyroblasts (0.1 mm in size) are present throughout the matrix (1–3 vol. %). The sericite abundance increases closer to the mineralized zone, and two generations of sericite are present, with an older, finer-grained generation that is oriented in the foliation and a younger, coarser-grained generation that is randomly oriented and overprints the foliation (Fig. 11d). Feldspar poikiloblasts are strongly chloritized, carbonatized, and locally biotitized. Some of the epidote grains probably formed syn- to late-deformation as they contain trails of gangue inclusions parallel to the main foliation (S_2) and are sometimes elongated parallel to the main foliation (Fig. 11e). Epidote is only present in the Zone 5 mineralized corridor, appearing a few meters from the footwall contact. Quartz, chlorite, and biotite are also aligned into the main foliation (S_2) (Fig. 11f). Two types of chlorite grains are present. The first type, accounting for 95 vol. % of the chlorite, occurs in the matrix and grains are less than 0.1 mm in size on average. A second, less common type of chlorite (5 vol. % of the chlorite present) occurs as near-total replacement of coarser biotite porphyroblasts (0.5 mm in size) and formed during retrograde metamorphism. Microprobe analysis confirmed that the chlorites present within the LZ5 mineralized corridors are of the ripidolite type, a basic magnesium iron aluminum silicate of the chlorite group. However, chlorites located in Zone 5 systematically have a higher Fe/(Fe+Mg) ratio. All of the carbonates analyzed from the LZ5 have typical ankerite compositions (Boily-Auclair et al., 2017). Compositional differences were not observed in carbonates according to their proximity to the mineralized zones. White micas analyzed under the microprobe are of the muscovite-type (Boily-Auclair et al., 2017).

Other mineral phases present in trace amounts (0.1–0.5 vol. %) in the proximal alteration halo in both the footwall and hanging wall of the LZ5 include zoisite, anhydrite, sphene, and tourmaline. Very fine disseminated ilmenite and coarser apatite grains are present throughout the mineralized zones of the LZ5.

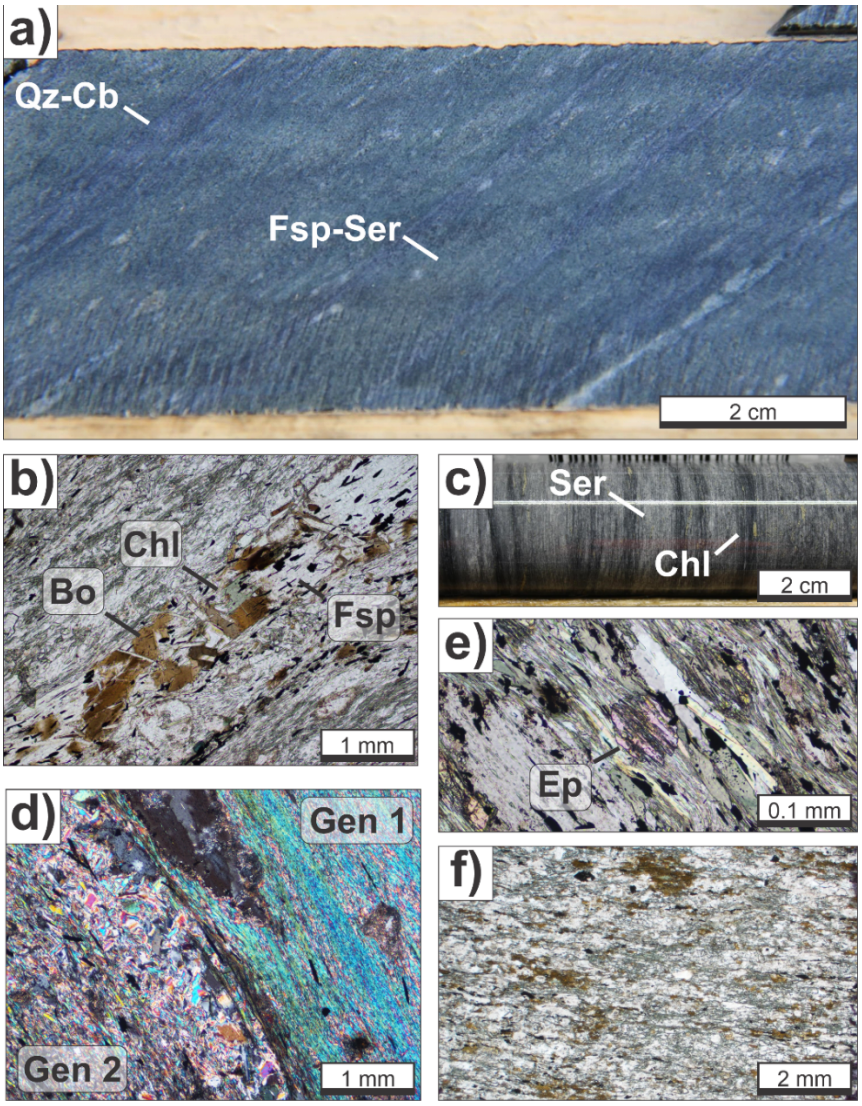

Figure 11. a) Distal banded sericite-carbonate-chlorite-quartz-feldspar assemblage developed in the Doyon basaltic-andesite (subunit 5.1a-(a)) and dacite-andesite (subunit 5.1a-(b)) of the LZ5 mineralized corridors. Note that the compositional bands are parallel to the S_2 fabric. Drillhole S11-44. Photograph by P. Mercier-Langevin, NRCan photo 2021-691. **b)** Photomicrograph (plane-polarized transmitted light) of a syndeformation feldspar porphyroblast elongated parallel to the main foliation (S_2) locally replaced by chlorite and biotite in the distal alteration assemblage of the LZ5 deposit, basaltic andesite volcanic rock (subunit 5.1a-(b)), drillhole S11-44. Photograph by E. Boily-Auclair, NRCan photo 2021-692. **c)** Intense proximal alteration assemblage in the vicinity of the LZ5 mineralized corridors consisting of sericite-dominated bands alternating with mm-wide chlorite and biotite-dominated bands. Drillhole BZ-1806136-1. Photograph by E. Boily-Auclair, NRCan photo 2021-693. **d)** Photomicrograph (cross-polarized transmitted light) of the intense proximal alteration assemblage, showing the two types of sericites observed within the mineralized corridors of the LZ5 deposit: 1) an older, finer-grained generation that is oriented in the foliation, and 2) a coarser-grained generation that is randomly oriented and overprints the foliation. Zone 5, drillhole S10-04. Photograph by E. Boily-Auclair, NRCan photo 2021-694. **e)** Photomicrograph (plane-polarized transmitted light) of an epidote grain in the intense proximal alteration assemblage of the LZ5 mineralized corridors. Note the presence of trails of gangue inclusion parallel to the main foliation (S_2) indicating a probable syn- to late deformation origin. Drillhole S11-44. Photograph by E. Boily-Auclair, NRCan photo 2021-695. **f)** Photomicrograph (plane-polarized transmitted light) of quartz, chlorite, and biotite aligned into the main foliation typical of the intense proximal alteration assemblage of the LZ5. Drillhole BZ-1805136-1. Photograph by E. Boily-Auclair, NRCan photo 2021-696.

Local proximal alteration assemblages

Within mineralized ore zones of the LZ5 deposit, a sericite-pyrite-quartz assemblage that forms meter-scale alteration corridors that contrast strongly with the surrounding host-rock of the LZ5 are well exposed in drill core and underground. These alteration corridors are characterized by sharp contacts, discordant cm-wide crosscutting faults, and high strain zones that give them the appearance of felsic sericite schists (Fig. 12a, b). They also contain up to 20 vol. % pyrite in the form of disseminations and small veinlets transposed into the main foliation. Traces of sphalerite and chalcopyrite are locally associated with these intense alteration zones. A detailed study of these intensely sericitized rocks made by Boily-Auclair et al. (2017) showed that, for the most part, they correspond to intermediate rocks that were intensely sericitized. However, one of the studied bands from Zone 4 corresponds to a felsic protolith (possibly a dyke) and is geochemically associated with the Westwood dacite-rhyodacite (subunit 5.1a-(d)).

The sericite-pyrite-quartz assemblage is characterized by a simple mineral assemblage composed of quartz and sericite with the presence of minor chlorite and carbonate (≤5 vol. %) locally. This local alteration contains garnet porphyroblasts that compose up to 5 vol. % of the rock (Fig. 12c). Similar to the epidote grains in the proximal alteration assemblage, trails of gangue inclusion parallel to the main foliation (S_2) are present within the elongated garnets and point toward a syn- to late-deformation timing for the formation of these porphyroblasts. These garnets are present in greater concentration in sericite-rich bands and can also be found in the immediate footwall and hanging wall of the sericite corridors. Garnet abundance and/or size do not appear to correlate with the presence of better Au grades.

Alteration Assemblages Associated with Zones A and B of the Ellison Property

Zone A at Ellison is predominantly hosted in intermediate volcanic rocks of the Bousquet Formation upper member, whereas Zone B is hosted in volcanic and volcaniclastic felsic rocks of the Westwood feldspar-phyric rhyolite dome (subunit 5.3a-(b)). The mineral alteration assemblages described for the ore zones of the Ellison property closely resemble the ones present at LZ5 and some of the alteration zones present at Westwood, west of the Ellison property (Wright-Holfeld et al., 2010, 2011; Yergeau, 2015; Yergeau et al., 2022a, b). Although the Ellison mineralized zones were not studied as thoroughly as the LZ5 ore zones in this study, alteration assemblages associated with zones A and B are briefly described here and compared with the alteration assemblages present at LZ5.

Ellison Zone A

The Ellison Zone A distal alteration can be traced up to 20 m on each side of the mineralized corridor in a N-S direction. It consists of a sericite-carbonate-quartz-feldspar ± chlorite-biotite assemblage that closely resembles the distal alteration developed in the intermediate units of the LZ5 mineralized zones (Fig. 12d). Millimeter- to cm-thick bands rich in quartz-carbonate alternate with bands rich in sericite ±feldspar. This alteration

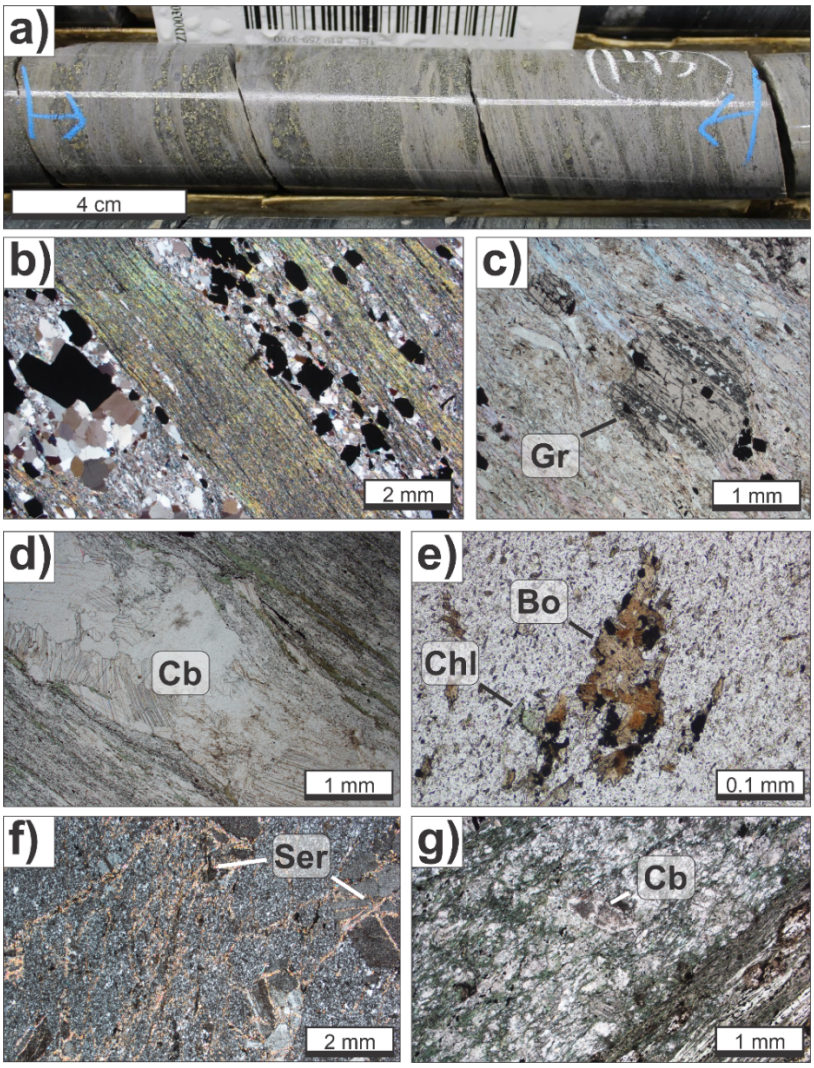

Figure 12. a) Proximal alteration assemblage in Zone 4 and Zone 5 of the LZ5 mine consisting mainly of a quartz-sericite-pyrite mineral assemblage that gives the rock a felsic appearance, dacite-andesite (subunit 5.1a-(b)) volcanic rock, drillhole BZ-1805136-1. Photograph by E. Boily-Auclair, NRCan photo 2021-697. **b)** Photomicrograph (cross-polarized transmitted light) showing the proximal alteration with bands composed almost exclusively of sericite aligned into the main foliation and bands of recrystallized quartz with granoblastic pyrite. Drillhole BZ-1805136-1. Photograph by E. Boily-Auclair, NRCan photo 2021-698. **c)** Photomicrograph (plane-polarized transmitted light) of garnet porphyroblasts in, or very close to, the proximal alteration assemblage. The garnets are syn- to late-deformation as they contain trails of gangue and inclusion minerals and are aligned into the S_2 foliation. Drillhole S11-44. Photograph by E. Boily-Auclair, NRCan photo 2021-699. **d)** Photomicrograph (plane-polarized transmitted light) of coarse recrystallized automorphic crystals of carbonates (up to 0.2 mm in size) aligned into the S_2 fabric. Proximal alteration assemblage of the Ellison Zone A observed in the Ellison intermediate volcanic unit, drillhole 121-06-11. Photograph by E. Boily-Auclair, NRCan photo 2021-700. **e)** Photomicrograph (plane-polarized transmitted light) of biotite retrograded to chlorite in proximity with the mineralized corridors of the Ellison Zone A, Ellison intermediate volcanic unit, drillhole 121-06-11. Photograph by E. Boily-Auclair, NRCan photo 2021-701. **f)** Photomicrograph (cross-polarized transmitted light) of fracture-controlled sericite observed within the volcaniclastic felsic unit (5.3a-(b)) hosting the Ellison Zone B mineralized corridors, drillhole 121-06-20. Photograph by E. Boily-Auclair, NRCan photo 2021-702. **g)** Distal alteration assemblage observed in the mafic unit composing the Ellison Zone B footwall consisting mainly of sericite, carbonate, and chlorite aligned in the S2 foliation, dacite-andesite (subunit 5.1a-(b)) volcanic rock, drillhole 121-06-11. Photograph by E. Boily-Auclair, NRCan photo 2021-703.

assemblage is characterized by a strong sericite alteration in which the foliation (S_2) is well developed. The sericite also locally replaces most of the feldspar present in the more mafic units of the footwall and, to a lesser extent, hanging wall. In the distal facies of the hanging wall of Zone A, carbonates appear as irregular, finely grained diffuse clusters that are generally up to 0.1 mm in size. In the footwall of Zone A, recrystallized quartz-carbonate amygdales with pyrite inclusions are distinctive (Mercier-Langevin, 2006). Chlorite and, very locally, biotite in sub-automorphic grains altered to chlorite may occur. Meters from the mineralized zones, in the footwall and hanging wall of Zone A, carbonates form coarse (up to 0.2 cm), recrystallized automorphic crystals (Fig. 12d). The sericite, chlorite, and carbonate content increase towards mineralized intervals. Within the mineralized zone, sericite, chlorite, and carbonate account for 40–50 vol. % of the rock. Carbonates are observed as coarse recrystallized grains (up to 0.2 cm) in association with the sulfide veins. Microprobe analysis revealed that the carbonates in the Ellison Zone A mineralized zone are also of the ankerite type (Lair, 2007).

Ellison Zone B

Two major alteration assemblages are associated with the felsic volcanic and volcaniclastic rocks of the Westwood feldspar-phyric rhyolitic dome (subunit 5.3a-(b)) in the Ellison Zone B corridor and its hanging wall: (1) a sericite-quartz-biotite ±feldspar-chlorite assemblage in the volcaniclastic unit and (2) a sericite-carbonate-quartz-feldspar-biotite-chlorite assemblage in the more massive volcanic unit. The fragments in the volcaniclastic rocks are composed almost exclusively of very fine-grained xenomorphic quartz whereas the matrix contains coarser, recrystallized xenomorphic to sub-automorphic quartz with up to 30 vol. % sericite. Some fragments are characterized by a compositional banding of quartz-rich bands and slightly sericitized, carbonatized, and silicified bands. Strongly sericite-altered feldspars are also present in the quartz-rich bands. The feldspar-rich volcanic facies is composed of a very fine-grained quartz matrix with feldspar and biotite phenocrysts. The biotite becomes more abundant towards the mineralized zone and is locally altered (retrograded) to chlorite (Fig. 12e). Feldspars are sericite altered. Sericite is well developed, fine-grained, and seems to be fracture-controlled (Fig. 12f). Closer to mineralization, the relative abundance of sericite, biotite, and chlorite increases, while quartz becomes less abundant. Up to 15 vol. % of chlorite and 15 vol. % of biotite is present close to the sulfide zone. The alteration minerals are elongated parallel to the well-developed foliation (S_2) in both massive and fragmental facies.

The Ellison Zone B footwall is principally composed of intermediate volcanic and volcaniclastic rocks of the upper member of the Bousquet Formation. The distal alteration assemblage in the intermediate rocks closely resembles the one observed in Zone A and at LZ5. The alteration assemblage principally consists of sericite, carbonate, and chlorite (Fig. 12g). Sericite is present as small sub-automorphic grains (>0.1 mm) disseminated through the matrix and is aligned into the S_2 fabric. The white micas represent between 20 and 40 vol. % of the alteration assemblage (Nadim, 2007). The carbonate relative abundance increases towards the mineralized zones and consists of large automorphic crystals (<0.1 mm) in proximity to the ore zones to small (>0.05 mm) scattered and diffuse xenomorphic

clusters (Nadim, 2007). Chlorite decreases in abundance towards the ore zone. Chlorite makes up to 25 vol. % of the alteration in the mineralized zone. It is xenomorphic to sub-automorphic and aligned into the foliation (Nadim, 2007).

ALTERATION INDICES AT LARONDE ZONE 5 AND ELLISON

Geochemical alteration indices can be used in mineral exploration to better define the geometry of hydrothermal systems, particularly in the case of VMS deposits, including those of the DBL camp (e.g., Mercier-Langevin, 2005; Wright-Holfeld, 2010, 2011; Dubé et al., 2014; Yergeau, 2015). Among the indices frequently used are: (1) the AI (or Hashimoto) index of Ishikawa et al. (1976) which represents the addition of MgO and K_2O by chloritization and sericitization of the rock and the loss of CaO and Na_2O by the destruction of feldspar and volcanic glass ($AI = 100*(MgO+K_2O)/(MgO+K_2O+CaO+Na_2O)$); (2) the modified chlorite-carbonate-pyrite index (CCPI) of Large et al. (2001) which represents the addition of MgO and $Fe_2O_3^{(t)}$ by pyritization, chloritization and carbonatization of the rock as well as the loss of K_2O and Na_2O by the destruction of feldspar and sericite ($CCPI = 100*(MgO+Fe_2O_3^T)/(MgO+Fe_2O_3^T+Na_2O+K_2O)$); and (3) the advanced argillic alteration index (AAAI) of Williams and Davidson (2004) which represents the leaching of MgO, CaO and Na_2O caused by the destruction of chlorite, carbonate, and feldspar by acidic fluids ($AAAI = 100*SiO_2/(SiO_2+(10*MgO)+(10*CaO)+(10*Na_2O))$).

Two geochemical profiles were created using these three alteration indices along drill holes S11-44 and 121-06-11, the longest and most representative drill holes of the ore zones under study (Figs. 13, 14). Borehole S11-44 crosscuts the LZ5 deposit from north to south in its entirety, while borehole 121-06-11 crosscuts the Ellison zones A and B.

In the vicinity of the mineralized zones of the LZ5 deposit, the AI and AAAI indices increase slightly, while the CCPI index remains relatively stable when compared to the adjacent fresh rocks (Fig. 13). The increase in AI and AAAI is related to the gain in potassium and to sodium leaching, in agreement with the development of a strong sericite alteration towards the mineralized intervals. In the ore zones, and more particularly within Zone 4, a local decrease of the CCPI index is present. However, the mineralization style of the LZ5 deposit (i.e., mm to cm-thick pyrite veinlets and disseminated pyrite) should cause an increase in the CCPI index due to the increase in iron due to pyritization. The local decrease in CCPI can be explained by the leaching of sodium directly in the mineralized zones by sericite alteration that compensates for the increase in iron by pyritization, especially in Zone 4, where m-wide, intensely sericite-altered bands are present (Fig. 13).

In the Ellison Zone B, an increase in the AI and AAAI indices, as well as a slight increase in the CCPI index appear when entering the mineralized zone (Fig. 14), in agreement with the greater abundance of pyrite. The sericitization in the Ellison Zone B is less intense than in the LZ5, and the leaching of sodium does not compensate for the increase in iron content. However, in the Ellison Zone A, a local high-grade Au sample is characterized by a significant increase in the AI and AAAI indices and a sharp decrease in

the CCPI index, similar to what is developed in the LZ5 mineralized zones. Intensely sericite-altered bands are present in the Ellison Zone A and could explain this signature.

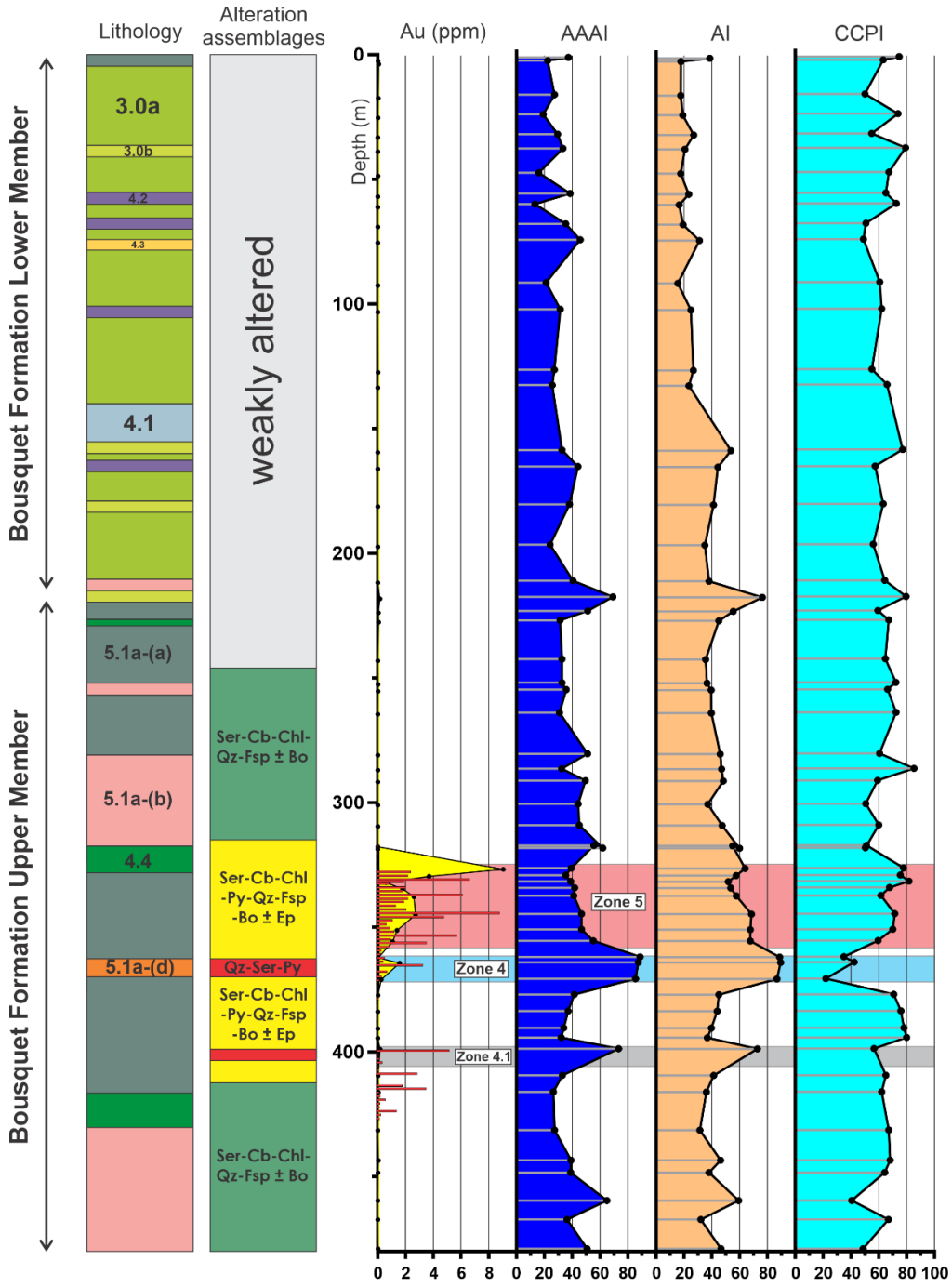

Figure 13. Geochemical profile along drillhole S11-44 that crosscuts the LZ5 deposit ore zones. Location of samples and geochemical data are shown by short horizontal lines. Red bars in the Au column represent assays from Agnico Eagle Mines Limited. Abbreviations: AAAI = advanced argillic alteration index ($100*((SiO_2)/(SiO_2+10MgO+10CaO+10Na_2O)$: Williams and Davidson, 2004). AI = Hashimoto alteration index ($100*(MgO+K_2O)/(MgO+K_2O+CaO+Na_2O)$): Ishikawa et al., 1976). CCPI = chlorite-carbonate-pyrite index ($(100*(MgO+Fe_2O_3^T)/(MgO+Fe_2O_3^T+Na_2O+K_2O)$: Large et al., 2001).

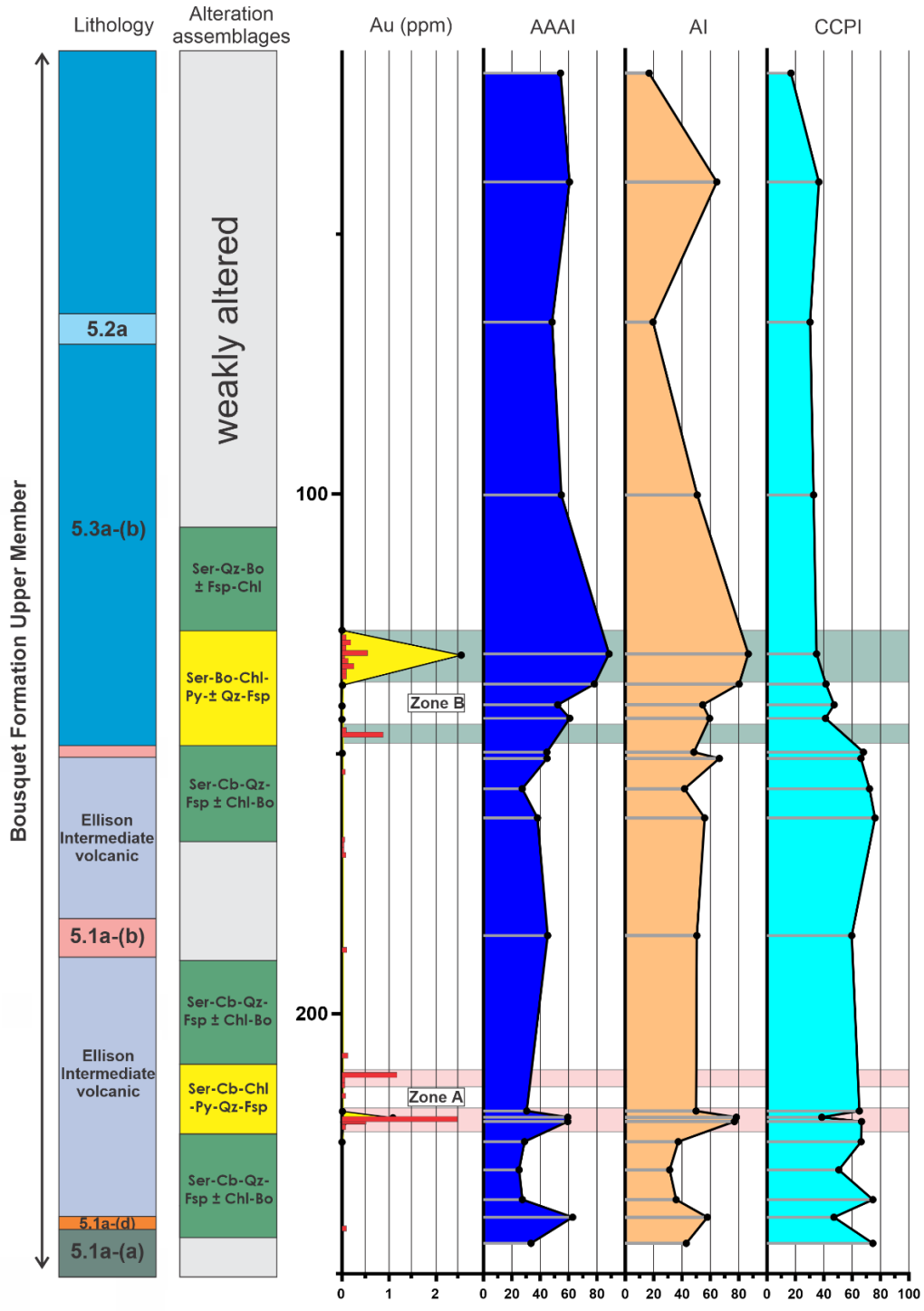

Figure 14. Geochemical profile along drillhole 121-06-11 on the Ellison property. Location of samples and geochemical data are shown by short horizontal lines. Red bars in the Au column represent assays by Agnico Eagle Mines Limited. Abbreviations: AAAI = advanced argillic alteration index ($100*((SiO_2)/(SiO_2+10MgO+10CaO+10Na_2O)$: Williams and Davidson, 2004). AI = Hashimoto alteration index ($100*(MgO+K_2O)/(MgO+K_2O+CaO+Na_2O)$: Ishikawa et al., 1976). CCPI = chlorite-carbonate-pyrite index ($(100*(MgO+FeO*)/(MgO+FeO*+Na_2O+K_2O)$: Large et al., 2001).

MASS CHANGES IN THE LARONDE ZONE 5 AND ELLISON ORE ZONES

Mass Changes

The single precursor mass balance calculation method of MacLean and Kranidiotis (1987) and Barrett and MacLean (1994) was used to calculate mass changes in the altered host rocks of the LZ5 and Ellison mineralized zones. This method requires two assumptions to be made: (1) monitor elements (e.g., Zr) are immobile and incompatible during fractionation in all rock types (mafic to felsic) of all magmatic affinities (tholeiitic to calc-alkaline) of the Bousquet and Ellison properties, and (2) the analyzed suite of samples includes both the protoliths (fresh or "least-altered" rocks) and representative examples of the alteration assemblages. About the second criterion, because least-altered samples are difficult to find at LZ5 (drilling and underground exposure are proximal to the mineralized zones and their alteration envelope), the composition of the host units was taken from Yergeau (2015) from the nearby Westwood deposit. Therefore, the suitability of the Westwood deposit area least-altered samples as precursors also had to be considered for the mass change calculations at LZ5. Mercier-Langevin (2005) and Yergeau (2015) established a way to properly identify least-altered samples in the Bousquet Formation using a series of specific criteria: (1) low loss on ignition values (<5 wt. %); (2) low concentration in S (<0.9 wt. %) and CO_2 (<2.5 wt. %); (3) total major element content close to 100%; as well as (4) a specific range of alteration indices (i.e. Hashimoto alteration index (AI: Ishikawa et al., 1976) ≤60; advanced-argillic alteration index (AAAI: Williams and Davidson, 2004) ≤60; and the modified chlorite-carbonate- pyrite index (CCPI: Large et al., 2001) ≤90). Using this approach, they were able to document the least-altered composition of most units and subunits of the Bousquet Formation. For the newly described intermediate volcanic unit hosting the Ellison Zone A on the Ellison property, the Bousquet heterogeneous unit (unit 4.4) photolith composition from Yergeau (2015) was used as they share a very similar geochemical composition. The mass change for this unit (Ellison volcanic intermediate unit) presented below must however be considered as a rough estimate since the primary composition of the host unit could not be fully characterized.

Aluminum, Zr, Ti, high-field strength trace elements (HFSE), and rare earth elements (REE) are usually immobile in hydrothermal alteration conditions typical of VMS systems and other systems dominated by moderate temperature (~200-400°C) and near-neutral pH (MacLean and Barrett, 1993). It is necessary to plot pairs of elements on bivariate diagrams to test their immobility within a specific system. An immobile element pair will plot on a common regression line that passes through the origin, with a high correlation coefficient (i.e. r = 0.9–0.99: MacLean and Barrett, 1993). Correlation coefficients can therefore be used to determine the most immobile (or least-mobile) element(s) during hydrothermal alteration of a volcanic rock sequence (MacLean and Kranidiotis, 1987). A series of binary diagrams were made to verify the immobility of elements normally considered as immobile to weakly mobile (i.e. Al_2O_3 and TiO_2, as well as, Hf, Nb, Y, and Zr) in unit 5.1a-(a) (Fig. 15a, b, c, d, e). Na_2O, a mobile oxide, is also plotted for comparison (Fig. 15f). Unit 5.1a-(a) was chosen for three main reasons: (1) the significant number of whole-rock analyses acquired from this unit (94 analyzed samples);

(2) unit 5.1a-(a) is the main host unit of the LZ5; and (3) unit 5.1a-(a) has probably undergone the most severe hydrothermal alteration of all the units in the study area. Zirconium and Hf were determined as the least mobile element pair in this study, and Zr was chosen as the monitor element as it is present in much higher concentrations in volcanic rocks than Hf (Fig. 15a) (Finlow-Bates and Stumpfl, 1981; Yergeau, 2015; Yergeau et al., 2022a, b).

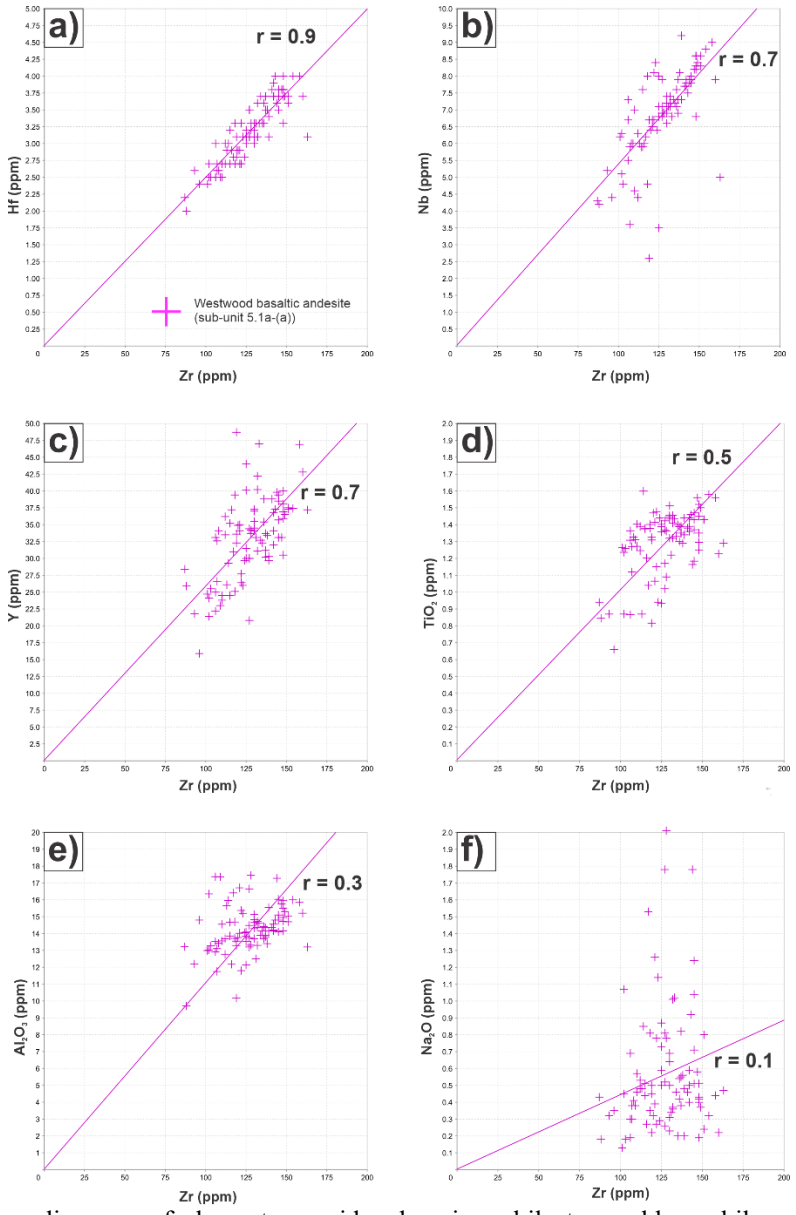

Figure 15. Binary diagrams of elements considered as immobile to weakly mobile used to verify the magmatic incompatibility and their immobility during alteration and metamorphism on the Bousquet and Ellison properties. The Westwood basaltic andesite (unit 5.1a-(a)) is illustrated. **a)** Hf-Zr binary diagram. **b)** Nb-Zr binary diagram. **c)** Y-Zr binary diagram. **d)** TiO_2-Zr binary diagram. **e)** Al_2O_3-Zr binary diagram. **f)** Na_2O-Zr binary diagram. Hf and Zr showed the best correlation with an r of 0.9 (almost linear). Zirconium was chosen as the monitor element for mass-change calculations.

Major Elements Mass Changes

The mass change values generated are used to develop profiles along drill holes to illustrate the effect of hydrothermal alteration on the units hosting the LZ5 and Ellison's mineralized zones in space (Figs. 16, 17). The distal alteration halo of the LZ5 is characterized by gains in CaO, CO_2, K_2O, MnO, and SiO_2 and locally MgO. In close proximity (≤5 m) and within the ore zones, gains in $Fe_2O_3^{(t)}$, K_2O, and TiO_2 and weak losses in Al_2O_3, CaO, MgO, Na_2O, and locally SiO_2 are distinctive (Fig. 16). The Ellison Zone A footwall shows gains in Al_2O_3, CaO, and K_2O and losses in $Fe_2O_3^{(t)}$ and Na_2O (Fig. 17). Mass changes in the Ellison Zone A hanging wall could not be properly evaluated due to a lack of data. Within the ore zone, leaching in CaO, Na_2O, SiO_2, TiO_2, and lesser MnO and MgO is characteristic. On the other hand, Al_2O_3, $Fe_2O_3^{(t)}$, and K_2O were added (Fig. 17). The Ellison Zone B mineralized corridor shows slightly different major element mass changes due to the felsic composition of its host rocks. The mineralized corridors are characterized by gains in $Fe_2O_3^{(t)}$ and local gains in K_2O, MgO, and MnO. Leaching of CO_2, Na_2O, P_2O_5, and SiO_2 is also present (Fig. 17). Table 2 presents the average, minimum and maximum mass changes for selected elements and oxides of the LZ5. Zirconium, Hf, Nb, and the REE are the most resistant to alteration. Sulfur showed the greatest mobility, along with CO_2, K_2O, MnO, $Fe_2O_3^{(t)}$, Na_2O, and metals such as Cr, Ni, and Co (Table 2). In general, LREE are more susceptible to hydrothermal alteration than HREE in the study area, as shown in Table 2.

DISCUSSION

The following section presents a summary of the research on the LZ5 deposit and discusses key elements, including the relative timing of events, the condition and potential nature of the hydrothermal fluids, and a geological model. The LZ5 and Ellison mineralized zones do not represent typical Archean Au systems as they primarily consist of stratabound to locally discordant sulfide veins, veinlets, and disseminations that contrast strongly with the more common quartz-carbonate vein, massive sulfide lenses, and intrusion-associated type deposits.

Relative Timing of Events

Our observations at LZ5 and Ellison indicate that sulfide deposition is related to the synvolcanic hydrothermal alteration episode(s) that predates regional metamorphism and the main phase of deformation. Sulfide-rich lapilli and blocks are present in the footwall rocks of the LZ5 mineralized corridors, indicating that some hydrothermal activity had started before the units of the upper Bousquet Formation were emplaced in the LZ5 and Ellison area. The presence of sulfide-filled amygdales in some of the volcanic units present in the footwall of the LZ5 also supports an early, pre-deformation and pre-metamorphic mineralizing event as vesicles are not left empty during seafloor diagenesis and hydrothermal alteration. More specifically, evidence for an early, pre-deformation, and possibly synvolcanic mineralization at LZ5 and Ellison includes: 1) major deformation and recrystallization of the sulfides and associated alteration assemblages; 2) the overall geometry of the ore zones and associated alteration halos (i.e. stacked mineralized lenses

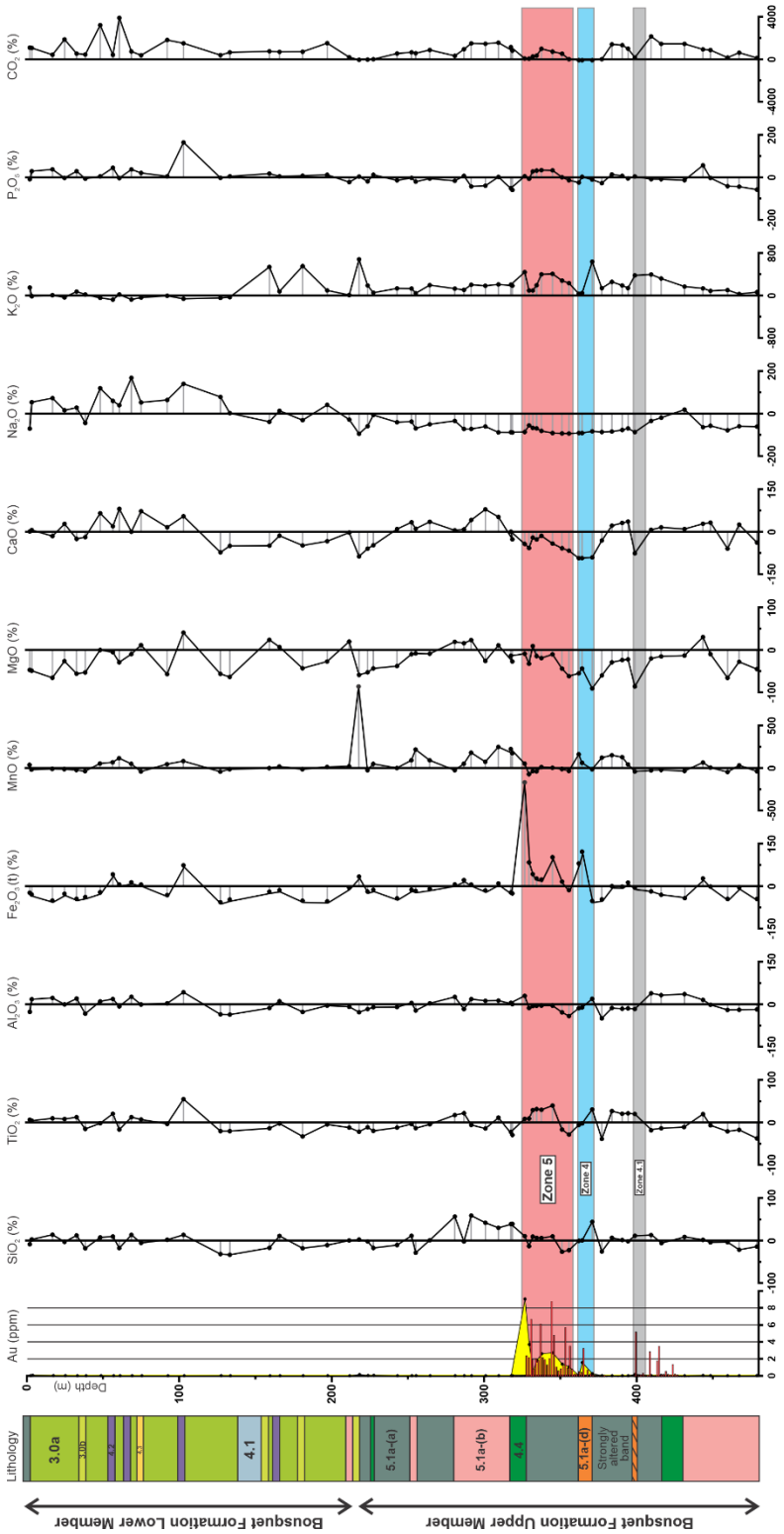

Figure 16. Major-oxide relative mass changes along drillhole S11-44. Mass gains and losses are shown on right and left sides of the middle line, respectively. Locations of samples and geochemical data are shown by short horizontal lines. Red bars in the Au column represent assays by Agnico Eagle Mines Limited.

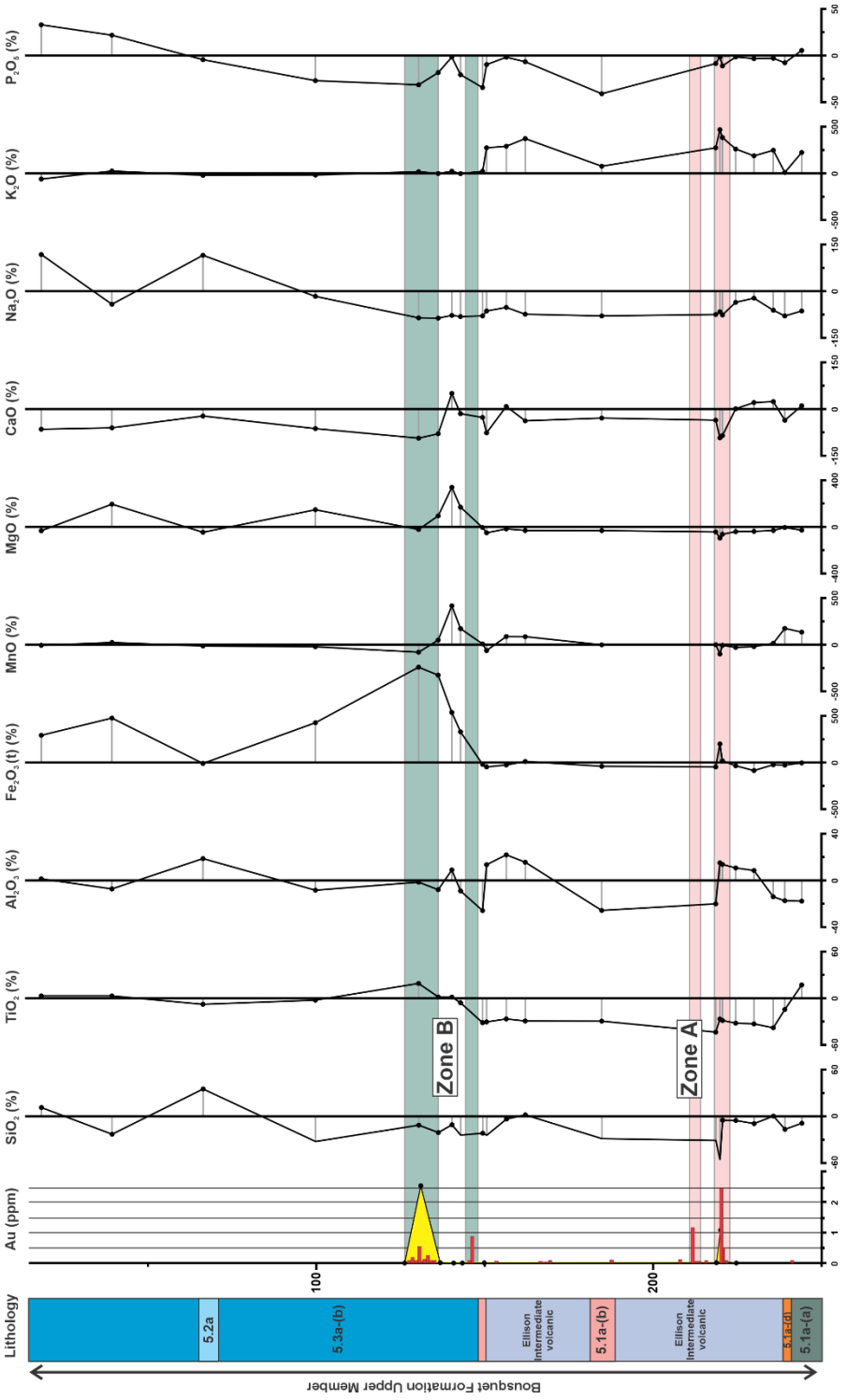

Figure 17. Major oxide relative mass changes percentages of the Ellison property along drillhole 121-06-11. Mass gains and losses are shown on right and left sides of the middle line, respectively. Locations of samples and geochemical data are shown by short horizontal lines. Red bars in the Au column represent assays by Agnico Eagle Mines Limited.

in a volcanic succession and subconcordant alteration halos); and 3) the emplacement of the mineralized zones controlled by volcanic features such as the permeability and porosity of the volcanic rocks and lithological contacts.

At LZ5, as in other parts of the DBL camp, deformation and metamorphic recrystallization largely obliterated the volcanic textures and alteration features that might have helped in the classification of its atypical mineralized corridors. This means that the current distribution and mineralogy of the mineralized zones and alteration envelopes do not necessarily reflect their primary distribution and characteristics. Nevertheless, it is still possible to define vectors towards the ore, reconstruct the original zonation in the system and discuss the possible nature of the hydrothermal fluids at the origin of the different mineralized corridors. For example, Boily-Auclair et al. (2020) have shown that the mineralized corridors appear at a specific stratigraphic position. They discuss the possibility that the complex intercalation of rock units present in the Bousquet and Ellison properties (i.e. tholeiitic to calc-alkaline, mafic to felsic, volcanic, volcaniclastic, and intrusive rocks) may have played a key role in the style, geometry, and metal budget of the ore-forming system of the LZ5 and Ellison ore zones.

The metamorphic recrystallization at LZ5 is evidenced by the mosaic texture of the pyrite, which presents pseudo-hexagonal recrystallized grains with junctions at 120° (Tourigny et al., 1992) (Fig. 8d). Tourigny et al. (1992) also suggested that fine tellurides inclusions, sphalerite, and chalcopyrite in the pyrite had probably been trapped during metamorphic recrystallization of the pyrite. Thus, the deposition of the necessary elements to form these mineral inclusions predates metamorphic recrystallization at upper-greenschist facies (Tourigny et al., 1992). Importantly, most of the veins are strongly folded, transposed, and boudinaged into the S_2 fabric (Fig. 8e, f). Shreds or boudins of dismembered veins and veinlets into the foliation are also common in underground mining stopes. These observations are evidence for a pre-deformation (D_2), pre-metamorphic (M_1) deposition of sulfides.

The LZ5 and Ellison mineralized zones share some similarities with the other synvolcanic deposits in the DBL camp. However, there are also significant differences that provide insight into the formation of the LZ5 and Ellison ore zones. The most notable differences are the absence of massive sulfide lenses and the relative depletion in base metals (Zn-Pb-Cu) and Ag when compared with more ‘’traditional’’ hydrothermal synvolcanic deposits of the camp. Base metals in VMS deposits are leached from the footwall rocks by hydrothermal fluids and deposited in massive sulfide bodies on the seafloor and/or below it (e.g., Franklin et al., 2005 and references therein). An influx of magmatic fluid and/or efficient precipitation mechanisms can also enrich these synvolcanic deposits in precious metals, as proposed for the LaRonde Penna, Bousquet2-Dumagami, and Westwood Au-rich VMS deposits (Mercier-Langevin, 2005; Dubé et al. 2007; Mercier-Langevin et al. 2007a, b; Dubé et al., 2014; Yergeau, 2015; Yergeau et al., 2022a, b). Due to the nature of the deposits in the DBL mining camp (i.e., Au-rich VMS, Au-rich sulfide veins, stockworks, disseminations, and intrusion-associated Au ±Cu veins), the LZ5 and Ellison deposits are probably part of a long-lived, large-scale hydrothermal system that

includes major synvolcanic Au mineralization (Dubé et al., 2014; Yergeau, 2015; Mercier-Langevin et al., 2017; Yergeau et al., 2022a, b).

An important aspect related to the timing of Au mineralization at LZ5 is provided by features that are compatible with the main deformation event in the camp. Late, discordant, sub-horizontal and locally Au and sulfide-bearing cm to dm-thick quartz-carbonate veins (syn- to late-D_2 extension veins) crosscut at high-angle the broad sulfide vein and disseminated-style mineralized zones at both LZ5 and Ellison. These veins are auriferous only when they intersect the altered and mineralized corridors of the LZ5 and Ellison deposits and are barren outside of the sulfide envelopes. This indicates that the formation of these syn- to late-D_2 quartz veins does not result in a new contribution of precious and base metals during deformation, but is rather due to local remobilization of metals already present within the LZ5 and Ellison mineralized corridors when the syn- to late-D_2 veins were emplaced.

Despite the fact that the ore zones at LZ5 and Ellison are greatly affected by superimposed, younger deformation episodes, mineralization at LZ5 and Ellison is pre-tectonic based on the elements presented above. Although some studies concluded that Au might have been introduced during deformation and metamorphism in the DBL camp deposits (e.g., Tourigny et al., 1988, 1989a, b, 1992; Marquis et al., 1990a, b), our interpretation is in agreement with some of the earliest interpretations (e.g., Valliant and Barnet, 1982; Valliant and Hutchinson, 1982; Valliant et al., 1982, 1983) and the most recent interpretations for many of the deposits of the camp (Stone, 1990; Dubé et al., 2004, 2014; Mercier-Langevin et al., 2007a, b, c, 2011, 2017; Yergeau, 2015; Yergeau et al., 2022a, b).

Conditions and Nature of the Alteration at the Bousquet and Ellison Properties

The LZ5 and Ellison ore zones are hosted in the upper member of the Bousquet Formation. Zone 4, Zone 4.1, and Zone 5 of the LZ5 deposit are hosted in subunits 5.1a-(a) and 5.1a-(b), which are transitional to calc-alkaline in magmatic affinity and intermediate in composition (Fig. 6a, b, c). The Ellison Zone A is hosted within a newly described intermediate calc-alkaline volcanic unit of the Bousquet Formation upper member, while the Ellison Zone B is hosted within subunit 5.3a-(b) of felsic nature and calc-alkaline affinity (Fig. 6a, b, c). The chemical changes resulting from the hydrothermal alteration are similar, for the most part, from one mineralized zone to another, but the initial composition of the host protolith influences the mineralogy of the alteration assemblages as well as the final chemical composition of the altered rocks.

The proximal hydrothermal alteration associated with these ore zones forms relatively symmetrical envelopes around the mineralization and extends at most a few meters out of the mineralized corridors, whereas the distal alteration assemblages extend tens of meters in the hanging wall and the footwall of the ore zones (Fig. 10). The alteration gradually increases in intensity towards the mineralized zones. This symmetry could be explained by the proximity of the different stacked mineralized corridors present on the Bousquet property. The LZ5 hanging wall is situated less than 50 m north of the Bousquet

1 Zone 3 footwall. Consequently, the distal alteration footprint in the Bousquet 1 Zone 3 footwall could have influenced the intensity of the alteration present in the LZ5 hanging wall. Similar to the Westwood deposit, the semi-conformable nature of the alterations around the LZ5 ore zones could also be explained by the diffuse fluid circulation caused by the volcaniclastic (permeable) nature of the host rocks. The intense N-S shortening during D_2 deformation probably accentuated the symmetrical aspect of the alteration halo. The distal footprint of the LZ5 and Ellison Zone A closely resembles "propylitic-style" alteration, which is common in hydrothermal deposits. Propylitic alteration (*sensu lato*) results from low to intermediate temperatures (200-350°C) and low fluid/rock ratios (Pacey et al., 2016). The metamorphosed alteration consists of a sericite-carbonate-chlorite-feldspar ±biotite assemblage with a distinctive Na-depletion and CaO, CO_2, and SiO_2 enrichment halo around the mineralized zones, typical of hydrothermal alteration related to VMS deposits (Figs. 11 a, b, 12d, 13) (Franklin et al., 1981; Galley and Lafrance, 2007).

In the vicinity of, and within, the mineralized zones, the alteration assemblage consists of a sericite-carbonate-chlorite-pyrite-quartz-feldspar-biotite ±epidote assemblage (Fig. 11c, d, e, f). The amount of disseminated pyrite also increases closer to the LZ5 and Ellison mineralized zones. This alteration assemblage could represent the remnant of a metamorphosed "sericitic-style" alteration, as suggested by the leaching of CaO and Na_2O, and by K_2O gains (Fig. 16) (Pacey et al., 2016). The loss of MgO within the ore zones of the LZ5 could have affected the chlorite composition which is Mg-rich outside of the LZ5 and Mg-poor within the mineralized corridors. Local very intense proximal alteration corridors consisting of a sericite-pyrite-quartz assemblage in zones 4 and 5 at LZ5 strongly contrast with the surrounding rocks (Fig. 12a, b). This alteration assemblage is characterized by a strong to total leaching of most major elements, except for $Fe_2O_3^{(t)}$, K_2O, SiO_2, Al_2O_3,and TiO_2 (Fig. 16). This intensely altered band is also characterized by a sharp increase of the AAAI and AI indices and a sharp decrease of the modified CCPI index, indicating leaching of CaO and Na_2O and addition of MgO and $Fe_2O_3^{(t)}$ (AAAI: Williams and Davidson, 2004; AI: Ishikawa et al., 1976; CCPI: Large et al., 2001) (Fig. 13).

Geological Model for the Formation of the LZ5 Deposit

Hannington et al. (1999) recognize two main mechanisms responsible for generating Au-rich deposits in the VMS environment: 1) an influx of Au-rich magmatic fluids and 2) boiling of hydrothermal fluids that allows for more efficient precipitation of Au from solution. Moreover, the presence of certain metals such as Bi in the hydrothermal fluids that drive VMS deposits is also recognized as a facilitating agent for Au transport and precipitation (e.g., Tormanen and Koski, 2005; Tooth et al., 2008; Mercier-Langevin et al., 2014). The lack of specific association between Au and anomalous trace metal contents in the LZ5 ore zones suggests that no specific ligand or scavenger element played a role in the formation of the LZ5 and Ellison Au-rich sulfide zones.

Beaudoin et al. (2014) conducted a detailed isotopic study on the LaRonde Penna 20 North and 20 South massive sulfide lenses. They proposed that the fluid temperatures were on the orders of 150°C, favoring the hypothesis for a cold, reduced, relatively acidic, and thiocomplexes-bearing fluid associated with the formation of the massive sulfide

lenses. Also, according to Beaudoin et al. (2014), the fluids responsible for the mineralization were a mixture between modified seawater and magmatic fluids. At LZ5 and Ellison, there is no evidence that hydrothermal fluids underwent boiling and/or phase separation (e.g., generation of vertical Cu-Au stockworks and stratiform Au-Zn-Pb-Ag ±Cu mineralized zones, and presence of stratiform clay alteration zones, or lithocaps), although this does not preclude the possibility that such processes happened.

An influx of Au-rich magmatic fluids, as proposed for the Bousquet 2-Dumagami, LaRonde Penna, and Westwood deposits (Dubé et al., 2007, 2014; Mercier-Langevin et al. 2007a–d, 2009, 2017; Beaudoin et al., 2014; Yergeau et al., 2022a, b), is plausible for LZ5. The magmas responsible for the emplacement of the volcanic and volcaniclastic rocks hosting the LZ5 and Ellison mineralized corridors, at the base of the Bousquet Formation upper member, are of transitional to calc-alkaline affinity. This means that the LZ5 ore is younger than the shift from tholeiitic to transitional, mafic to intermediate volcanic activity to more calc-alkaline activity (Boily-Auclair et al., 2020) (Fig. 18). This shift had been noted at the camp scale but did not appear to apply to the mineralization at LZ5 due to misinterpretation of its stratigraphic position (*see* Boily-Auclair et al., 2020). This transition is accompanied by an evolution of mineralization towards an Au-bearing VMS style higher in the stratigraphy, especially in the eastern part of the camp (Figs. 2, 3). According to Mercier-Langevin et al. (2007a), the magmas that formed the Bousquet Formation were formed by assimilation of crustal material and fractional crystallization (AFC) within a subsidiary magma chamber located in a thick, immature island arc or juvenile back-arc basin in an extensional geodynamic setting. This model was recently refined in Yergeau et al. (2022a). Alkaline and calc-alkaline magmas are known to be favourable for the transport of Au and other metals since they are generally oxidized and fluid-rich (Sinclair, 2007).

Although the presence of widespread advanced argillic-style alteration is considered a very good indicator of magmatic fluid input in VMS systems (e.g., Sillitoe et al., 1996; Dubé et al., 2014), its absence (as it is the case at LZ5) does not necessarily mean that magmatic fluids were not present (e.g., Hannington et al., 1999; Yergeau et al., 2022a, b). Indeed, magmatic fluids can react and equilibrate at greater depths with modified seawater and thus generate fluids whose pH and sulfidation state is intermediate between the two original fluids (Hannington et al., 1999). The synvolcanic Mooshla intrusion could also have played an important role in the Au-enrichment of the LZ5 and Ellison mineralized corridors. Galley and Lafrance (2014) noted the presence of miarolitic cavities containing chlorite, magnetite, pyrite, and chalcopyrite (±Au) in the late phases of the Mooshla pluton, indicating the exsolution of metal-rich fluids. The Doyon mine is also interpreted to be genetically associated with the pluton emplacement and the crystallization of its different phases (Gosselin, 1998; Galley and Lafrance, 2007, 2014).

In summary, the mineralized zones of the LZ5 and Ellison deposits probably formed from the mixture of two fluids. The dominant one would have been modified, metal-enriched seawater circulating below the seafloor. The second fluid would have been magmatic fluids from dykes, sills, and cryptodomes of the upper member of the Bousquet Formation as well as from the upper portion of the Mooshla pluton (or a parent magmatic

chamber at depth). Although its size at the current surface is small, the Mooshla intrusive complex may represent the shallower equivalent of a much larger intrusive body that could have helped drive hydrothermal activity in the DBL mining camp (Valliant and Hutchison, 1982; Mercier-Langevin et al., 2007d; Dubé et al., 2007; Galley and Lafrance, 2014; Yergeau, 2015). The low base metal content at LZ5 could be explained by the greater influx of magmatic fluids in the hydrothermal system that formed the mineralized ore zones. The mineralized zones of the LZ5 deposit are also enriched in Ba, Bi, Cu, In, Sn, Te, and slightly enriched in Ag, Se, and W. The Ellison Zone A shows similar metal enrichment, with the addition of As, Co, and Pb. The Ellison Zone B is additionally enriched in Cd, Hg and Zn. Although not necessarily a diagnostic feature, enrichment in trace elements such as Ag, As, Bi, Hg, Sn, and Te is associated with a magmatic-input into ore-forming hydrothermal systems, in agreement with the Au ±Cu-rich nature of some of the deposits of the DBL camp (e.g., Dubé et al., 2004, 2007, 2014; Mercier-Langevin, 2005; Mercier-Langevin et al., 2007c, 2011; Yergeau, 2015; Yergeau et al., 2022a, b). The anomalous Au enrichment and the absence of advanced argillic-style alteration near the LZ5 deposit could therefore be explained by: (1) the proximity to a magmatic source (i.e. the Mooshla intrusive complex); and (2) a modified, metal-enriched seawater circulating by convection under the sea-floor.

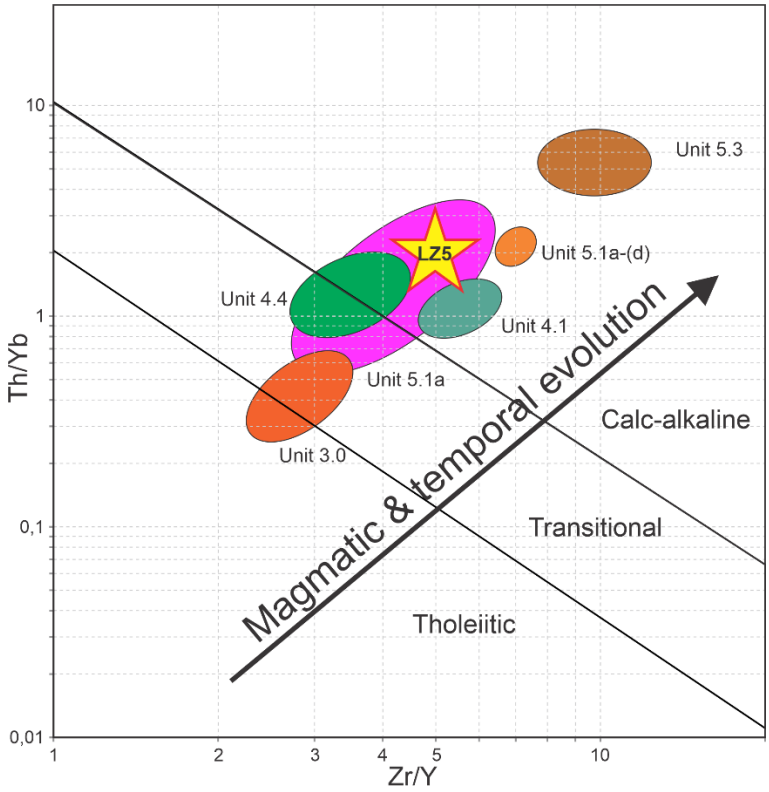

Figure 18. Temporal and magmatic evolution of the units composing the Bousquet Formation lower and upper members at LZ5 and Ellison. The transition from the Bousquet Formation lower member (units 1 to 4) to the Bousquet Formation upper member (units 5) marks a transition in the nature of magmatism that coincides with the onset of major Au-rich hydrothermal activity at LZ5 as elsewhere in the DBL mining camp. Th/Yb versus Zr/Y magmatic affinity diagram from Ross and Bédard (2009).

The Ellison Zone A is located at the same stratigraphic position as the LZ5 and is hosted in the newly described Ellison intermediate volcanic unit. Zone A could represent the distal part of the LZ5 Zone 4 mineralized corridor. The Ellison Zone B is located higher in the stratigraphic sequence, in felsic volcanic and volcaniclastic rocks of subunit 5.3a-(b) and could represent a distal expression of zones 1 and 2 at the former Bousquet 1 mine (Fig. 3). Although the Ellison zones A and B were not studied in great detail here, there are some differences between these mineralized zones and the LZ5 deposit. One of the most important differences is the presence of thin, semi-massive, and massive pyrite lenses (<30 cm) within the mineralized corridors of the Ellison Zone A and Zone B. The Au content is generally higher at Ellison (e.g., 3–6 g/t au over 1 m), but the ore zones are laterally less continuous, and thinner (e.g., 1–6 m wide). However, much more work would be needed on the Ellison property to properly characterize its ore zone and host unit.

The emplacement of the mineralization was controlled at least in part by the permeable nature of the host rocks (i.e. dominantly volcaniclastic rocks at the base of the upper member of the Bousquet Formation) allowing for diffuse mineralized fluid circulation. This could also explain the absence of a well-defined discordant narrow alteration pipe below the LZ5 and Ellison mineralized zones. There is no evidence to suggest that any part of the mineralized zone was formed by exhalative activity onto the seafloor.

The LZ5 could represent a sub-seafloor stockwork and replacement-style VMS-type system that however did not reach the necessary maturity to form massive sulfides. The low concentration of base metals (Cu and Zn) in the LZ5 mineralized system is perhaps due to the involvement of relatively cold (≤200°C) hydrothermal fluids that could not transport base metals. Similar to what has been proposed for the adjacent Westwood deposit, Au could have been introduced in the system by a magmatic influx from the Mooshla intrusive complex or a deeper-seated magmatic chamber. Aluminosilicate-rich acidic clay alteration, which is typical of the Bousquet 2-Dumagami deposit and the deep part of the 20N lens of the LaRonde Penna deposit, is absent at LZ5. Weaker magmatic fluid input, or more mixing with modified seawater, could have neutralized the acidic character of the fluid, explaining the absence of advanced argillic-style alteration at LZ5. However, metamorphosed argillic-style alteration is common along Zone 3, which sits a few tens of meters higher in the stratigraphy than the LZ5 ore zones. If these ore zones are all associated, then this means that the acidic character of the fluids could not be expressed, perhaps due to temperatures still slightly too elevated. Although this is a possibility, it is beyond the objectives of this research and will be discussed elsewhere. We, therefore, consider the LZ5 mineralization to represent a hybrid case between a “LaRonde-style” and a “Westwood-style” deposit, with an input of magmatic fluids and possibly metals to form a magmatic-hydrothermal system.

CONCLUSION

The detailed study of the LZ5 and Ellison Au-rich mineralized corridors has allowed to better constrains their characteristics and position in the metallogenic and petrogenetic evolution of the DBL mining camp. It also provides detailed documentation of a style of

Au mineralization that is often considered atypical as it is not as common as other Archean Au deposit styles. The unique characteristics of the LZ5 deposit (i.e. network of Au-rich pyrite veins and veinlets (stockworks); low base metal and Ag content; lack of massive sulphide lenses; and limited felsic rocks in the vicinity of the mineralized zones) has hindered its comparison with the known styles of mineralization in the camp. A major overprint by structural features related to the main phase of regional shortening (locally referred to as D_2) further complicated the study and understanding of Au emplacement in this part of the camp and led to conflicting interpretations in the past about the timing of ore-forming events.

The LZ5 is hosted at the base of the Bousquet Formation upper member, within transitional to calc-alkaline intermediate volcanic and volcaniclastic rocks of the Westwood basaltic-andesite (subunit 5.1a-(a)), and Westwood andesite-dacite (subunit 5.1a-(b)). The Ellison Zone A is hosted within an intermediate volcanic unit of calc-alkaline affinity (Ellison intermediate volcanic unit). This unit was previously not described on the Ellison property and is geochemically similar to the host units of the LZ5.

The Ellison Zone B is hosted within calc-alkaline felsic volcaniclastic rocks of the Westwood feldspar-phyric rhyolitic dome (subunit 5.3a-(b)). Unit 5.1a marks the transition from tholeiitic to transitional, to transitional to calc-alkaline, magmatism. The creation, emplacement, and crystallization of magmas of intermediate to felsic composition and transitional to calc-alkaline affinity appear to be important in generating an Au- rich magmatic-hydrothermal fluid that contributes to the enrichment of the various mineralized corridors of the Bousquet and Ellison property. The most permeable and porous units hosting the LZ5 and Ellison mineralized corridors are interpreted to have played an important role in the emplacement of the ore zones by allowing diffuse mineralized fluid circulation and precipitation of metals. Metamorphosed propylitic- and sericitic-style alterations are developed in the rock hosting the mineralized corridors of the LZ5 and Ellison Zone A. These subconcordant alteration halos are associated with the synvolcanic emplacement of the ore zones prior to regional deformation and metamorphic events. The intense shortening associated with the D_2 deformation event has folded, transposed, and boudinaged the Au-rich pyrite veins and veinlets network into the foliation. Remnants of veins transposed and dismembered into the foliation are common. Local remobilization of metals into sulfide and Au-rich quartz-carbonate veins is also locally present in the ore zones.

Despite superimposed deformation and metamorphism at LZ5, the primary characteristics of the mineralized zones and the host volcanic and intrusive rocks were still generally identifiable, which made it possible to reconstruct the pre-deformation geological history of the deposit and thus better characterize its synvolcanic origin, genesis, and architecture. The exploration for similar Au-rich Archean deposits should therefore focus on: (1) mafic to felsic (non-bimodal) volcanic and intrusive rock sequences of transitional to calc-alkaline affinity with one or more polyphase synvolcanic intrusions at a regional scale; (2) semi-conformable halos consisting of propylitic and sericitic-style alteration assemblages (i.e. sericite, chlorite, biotite, carbonates, and feldspar) characterized by large Na_2O-depletion and CaO, CO_2, and SiO_2 enrichment halo around the mineralized zones;

and (3) permeable (i.e. fragmental) facies within the intermediate, transitional to calc-alkaline differentiated volcanic rocks at a local scale.

ACKNOWLEDGMENTS

This report is part of an MSc thesis at the Institut national de la recherche scientifique, Centre Eau Terre Environnement, by the first author. The authors wish to thank Agnico Eagle Mines Ltd for access to the LaRonde Zone 5 deposit, access to drill cores and databases, and for sharing data and knowledge about the Doyon-Bousquet-LaRonde mining camp. The LaRonde Division and its personnel, in particular D. Fortin, R. Dubuc, D. Lussier, and M. Bernier, are thanked for their support and for numerous constructive discussions. This report is a contribution to the Targeted Geoscience Initiative Program (TGI) Gold Project and Orogenic Ore Systems Project of Natural Resources Canada. An earlier version of this report was reviewed by Dr. Benoît Dubé.

REFERENCES

Agnico Eagle Mines Limited, 2019. LaRonde Zone 5 survey division, Agnico Eagle Mines Limited, Map of level 18 of the LaRonde Zone 5 project, scale 1:1500.

Agnico Eagle Mines Limited, 2021. LaRonde mine operations, Agnico Eagle Mines Limited. < https://www.agnicoeagle.com/English/operations-and-development-projects/operations/laronde/default.aspx> [accessed June 19, 2021]

Ayer, J., Amelin, Y., Corfu, F., Kamo, S., Ketchum, J., Kwok, K. and Trowell, N., 2002. Evolution of the southern Abitibi greenstone belt based on U-Pb geochronology: autochthonous volcanic construction followed by plutonism, regional deformation and sedimentation; Precambrian Research, v. 115, p. 63-95.

Barrett, T.J. and MacLean, W.H., 1994. Chemostratigraphy and hydrothermal alteration in exploration for VHMS deposits in greenstones and younger volcanic rocks; *in* Alteration and alteration processes associated with ore-forming systems; Geological Association of Canada, Mineral Deposits Division, Short Course Notes, v. 11, p. 433–467.

Beaudoin, G., Mercier-Langevin, P., Dubé, B., and Taylor, B.E., 2014. Low-temperature alteration at the world-class LaRonde Penna Archean Au-rich volcanogenic massive sulfide deposit, Abitibi subprovince, Quebec, Canada: Evidence from whole-rock oxygen isotopes; Economic Geology, v. 109, p. 167-182.

Bleeker, W., 1999. Structure, stratigraphy, and primary setting of the Kidd Creek volcanogenic massive sulfide deposit: A semiquantitative reconstruction; *in* Monograph 10: The giant Kidd Creek volcanogenic massive sulfide deposit, Society of Economic Geologists, p. 71-122.

Boily-Auclair, E. 2017. Nature et style de l'altération hydrothermale associée aux minéralisations aurifères du projet LaRonde Zone 5 (LZ-5), Abitibi, Québec; Unpublished B.Sc. thesis, Université Laval, Québec, Quebec, 69 pages.

Boily-Auclair, E., Mercier-Langevin, P., Ross, P.-S., and Pitre, D., 2019. Lithological and structural controls on the nature and distribution of gold at the LaRonde Zone 5 Project, Doyon- Bousquet-LaRonde gold camp, Abitibi, Quebec; *in* Targeted Geoscience Initiative: 2018 report of activities, (ed.) N. Rogers; Geological Survey of Canada, Open File 8549, p. 23–32.

Boily-Auclair, E., Mercier-Langevin, P., Ross, P-S., and Pitre, D., 2020. Stratigraphic setting of the LZ5 and Ellison mineralized zones, LaRonde Zone 5 Project, Doyon-Bousquet-LaRonde mining camp, Abitibi, Quebec; *in* Targeted Geoscience Initiative 5, Gold Project: A summary of contributions to the understanding of Canadian gold systems; Geological Survey of Canada, Open File 8712, p. 57-73.

Calvert, A.J., Sawyer, E.W., Davis, W.J. and Ludden, J.N., 1995. Archaean subduction inferred from seismic images of a mantle suture in the Superior Province; Nature, v. 375, p. 670-674.

Chown, E.H., Daigneault, R. and Mueller, W.U., 1992. Tectonic evolution of the Northern Volcanic Zone, Abitibi belt, Quebec; Canadian Journal of Earth Sciences, v. 29, p. 2211-2225.

Clowes, R.M., Calvert, A.J., Eaton, D.W., Hajnal, Z., Hall, J. and Ross, G.M., 1996. Lithoprobe reflection studies of Archean and Proterozoic crust in Canada; Tectonophysics, v. 264, p. 65-88.

Davis, D.W., 2002. U-Pb geochronology of Archean metasedimentary rocks in the Pontiac and Abitibi subprovinces, Quebec: constraints on timing, provenance and regional tectonics; Precambrian Research, v.115, p. 97-117.

Dubé, B., Mercier-Langevin, P., Hannington, M., Davis, D.W. and Lafrance, B., 2004. Le gisement de sulfures massifs volcanogènes aurifères LaRonde, Abitibi, Québec : altération, minéralisations, genèse et implications pour l'exploration; Ministère des ressources naturelles et de la Faune du Québec; MB 2004-03, 112 pages.

Dubé, B., Mercier-Langevin, P., Hannington, M., Lafrance, B., Gosselin, G., and Gosselin, P., 2007. The LaRonde Penna world-class Au-rich volcanogenic massive sulfide deposit, Abitibi, Québec: mineralogy and geochemistry of alteration and implications for genesis and exploration; Economic Geology, v. 102, p.633–666.

Dubé, B., Mercier-Langevin, P., Kjarsgaard, I., Hannington, M., Bécu, V., Côté, J., Moorhead, J., Legault, M., and Bédard, N., 2014. The Bousquet 2-Dumagami world class Archean Au-rich volcanogenic massive sulfide deposit, Abitibi, Québec: metamorphosed submarine advance argillic alteration footprint and genesis; Economic Geology, v. 109, p.121–166.

Dubé, B. and Mercier-Langevin, P., 2020. Gold deposits of the archean Abitibi greenstone belt, Canada; *in* Geology of the world's major gold deposits and provinces; chapter 32, p. 669-708.

Franklin, J.M., Sangster, D.F. and Lydon, J.W., 1981. Volcanic-associated massive sulfide deposits; *in* Economic Geology 75th Anniversary Volume; Society of Economic Geologists, p. 485-627.

Franklin, J.M., Gibson, H.L., Jonasson, I.R. and Galley, A.G., 2005. Volcanogenic Massive Sulfide Deposits, *in* Economic Geology 100th Anniversary Volume; Society of Economic Geologists, p. 523-560.

Finlow-Bates, T. and Stumpfl, E.F., 1981. The behaviour of so-called immobile elements in hydrothermally altered rocks associated with volcanogenic submarine-exhalative ore deposits; Mineralium Deposita, v. 16, p.319-328.

Galley, A.G. and Lafrance, B., 2007. Évolution et métallogénie du Pluton de Mooshla; Ministère des Ressources naturelles, de la Faune et des Parcs, ET 2007-02, 32 p.

Galley, A.G., and LaFrance, B., 2014. Setting and evolution of the Archean synvolcanic Mooshla Intrusive Complex, Doyon-Bousquet-LaRonde Mining Camp, Abitibi Greenstone Belt: Emplacement History, Petrogenesis, and Implications for Au Metallogenesis; Economic Geology, v. 109, p. 205-229.

Gosselin, G., 1998. Veines de quartz aurifères précoces à la zone Ouest de la mine Doyon, Canton de Bousquet, Preissac, Abitibi; Mémoire de maitrise; Unité d'enseignement en sciences de la Terre, Université du Québec à Chicoutimi, Chicoutimi, 128 p.

Hubert, C., Trudel, P. and Gélinas, L., 1984. Archean wrench fault tectonics and structural evolution of the Blake River Group, Abitibi Belt, Quebec; Canadian Journal of Earth Sciences, v. 21, p.1024-1032.

Hannington, M.D., Poulsen, K.H., Thompson, J.F.H., and Sillitoe, R.H., 1999. Volcanogenic gold in the massive sulfide environment; Economic Geology, v. 13, p. 325-355.

Hubert, C., Trudel, P., and Gélinas, L., 1984. Archean wrench fault tectonics and structural evolution of the Blake River Group, Abitibi belt, Quebec; Canadian Journal of Earth Sciences, v. 21, p. 1024−1032.

Ishikawa, Y., Sawaguchi, T., Iwaya, S., and Horiuchi, M., 1976. Delineation of prospecting targets for Kuroko deposits based on modes of volcanism of underlying dacite and alteration haloes; Mining Geology, v. 26, p. 105–117.

Kirkland Lake Gold Limited, 2021. Detour Lake Mine; Kirkland Lake Gold Ltd < https://www.kl.gold/our-business/canada/detour-lake-mine/default.aspx> [accessed January 14, 2021].

Lafrance, B., Moorhead, J., and David, D.W., 2003. Cadre géologique du camp minier Doyon-Bousquet-LaRonde; Ministère des Ressources naturelles, de la Faune et des Parcs du Québec, ET 2002-07, 45 p.

Lafrance, B., Davis, D.W., Goutier, J., Moorhead, J., Pilote, P., Mercier- Langevin, P., Dubé, B., Galley, A.G., and Mueller, W.U., 2005. Nouvelles datations isotopiques dans la portion québécoise du Groupe de Blake River et des unités adjacentes; Ressources Naturelles et Faune Québec, RP 2005–01, 15 pages.

Lair, M. 2007. Caractérisation pétrographique et géochimique des altérations et des minéralisations aurifères de la Zone A, propriété Ellison, camp minier Doyon-Bousquet-LaRonde; Unpublished B.Sc. Thesis, Laval University, 33 pages.

Large, R. R., Gemmell, J. B., Paulick, H., and Huston, D. L., 2001. The alteration box plot: A simple approach to understanding the relationship between alteration mineralogy and lithogeochemistry associated with volcanic-hosted massive sulfide deposits; Economic Geology, v. 96, p. 957-971.

Marquis, P., Hubert, C., and Brown, A.C., 1990a. Gold deposits in deformed massive sulfide and pyretic alterites in the Bousquet district, southern Abitibi Subprovince; Short Course Notes; University of Western Australia, v.24, p. 243-273.

Marquis, P., Hubert, C., Brown, A.C., and Rigg, D.M., 1990b. An evaluation of genetic models for gold deposits of the Bousquet district, Quebec, based on their mineralogic, geochemical, and structural characteristics; *in* The Northwestern Quebec Polymetallic Belt: a summary of 60 years of mining exploration; CIM Special Volume 43, p. 383-399.

MacLean, W.H. and Kranidiotis, P., 1987. Immobile elements as monitors of mass transfer in hydrothermal alteration; Phelps Dodge massive sulfide deposit, Matagami, Quebec; Economic Geology, v. 82, p. 951-962.

MacLean, W.H. and Barrett, T.J., 1993. Lithogeochemical techniques using immobile elements; Journal of Geochemical Exploration, v. 48, p. 109-133.

McNicoll, V., Goutier, J., Dubé, B., Mercier-Langevin, P., Ross, P.-S., Dion, C., Monecke, T., Legault, M., Percival, J., and Gibson, H., 2014. U-Pb geochronology of the Blake River Group, Abitibi Greenstone Belt, Quebec, and implications for base metal exploration; Economic Geology, v. 109, p. 27–59.

Mercier-Langevin, P., 2005. Géologie du gisement de sulfures massifs volcanogènes aurifères LaRonde, Abitibi, Québec; Ph.D. thesis, Institut national de la Recherche scientifique – Centre Eau, Terre et Environnement, Québec, Quebec, 694 pages.

Mercier-Langevin, P., 2006. Campagne de forage – Propriété Ellison, Hiver 2006, Mines Agnico-Eagle Ltée, Division Exploration, Canton Bousquet, Abitibi, Québec ; Rapport déposé au Ministère des Ressources Naturelles et de la Faune, Juillet 2006, GM 62983, 305 pages.

Mercier-Langevin, P., Dubé, B., Hannington, M.D., Davis, D., Lafrance, B., and Gosselin, G., 2007a. The LaRonde Penna Au-rich volcanogenic massive sulfide deposit, Abitibi greenstone belt, Quebec: Part I. Geology and geochronology; Economic Geology, v. 102, p. 585–609.

Mercier-Langevin, P., Dubé, B., Hannington, M.D., Richer-Laflèche, M., and Gosselin, G., 2007b. The LaRonde Penna Au-rich volcanogenic massive sulfide deposit, Abitibi greenstone belt, Quebec: Part II. Lithogeochemistry and paleotectonic setting; Economic Geology, v. 102, p. 611–631.

Mercier-Langevin, P., Dubé, B., Lafrance, B., Hannington, M.D., Galley, A., and Moorhead, J., 2007c, A group of papers devoted to the LaRonde Penna Au-rich volcanogenic massive sulfide deposit, eastern Blake River Group, Abitibi greenstone belt, Quebec: Preface: Economic Geology, v.102, p. 577-583.

Mercier-Langevin, P., Dubé, B., Lafrance, B., Hannington, M., Galley, A., Moorhead, J., and Gosselin, P., 2007d. Metallogeny of the Doyon-Bousquet-LaRonde mining camp, Abitibi greenstone belt, Quebec; *in* Mineral Deposits of Canada: A Synthesis of Major Deposit Types, District Metallogeny, the Evolution of Geological Provinces, and Exploration Methods; Geological Association of Canada, Mineral Deposits Division, Special Publication No. 5, p. 673–701.

Mercier-Langevin, P., Wright-Holfeld, A., Dubé, B., Bernier, C., Houle, N., Savoie, A., and Simard, P., 2009. Stratigraphic setting of the Westwood-Warrenmac ore zones, Westwood Project, Doyon-Bousquet-LaRonde mining camp, Abitibi, Québec; Geological Survey of Canada, Current Research Paper 2009-3, 20 pages.

Mercier-Langevin, P., Hannington, M.D., Dubé, M., and Bécu, V., 2011. The gold content of volcanogenic massive sulfide deposits; Miner Deposita, v. 46, p. 509–539.

Mercier-Langevin, P., Gibson, H.L., Hannington, M.D., Goutier, J., Monecke, T., Dubé, B., and Houlé, M.G., 2014. A special issue on Archean magmatism, volcanism and ore deposits: Part 2. Volcanogenic massive sulfide deposits; Economic Geology, v. 109, p. 1–9.

Mercier-Langevin, P., Dubé, B., Blanchet, F., Pitre, D., and Laberge, A., 2017. The LaRonde Penna Au-rich volcanic-hosted massive sulfide deposit; Reviews *in* Economic Geology, v. 19, p. 225–245.

Mercier-Langevin, P., Lawley, C., Castonguay, S., Dubé, B., Bleeker, W., Pinet, N., Bécu, V., Pilote, J-L., Jackson, S., Wodicka, N., Honsberger, I., Davis, W., Petts, D., Yang, Z.,

Jautzy, J., and Lauzière, K., 2020. Targeted Geoscience Initiative 5, Gold Project: A summary of contributions to the understanding of Canadian gold systems; Geological Survey of Canada, Open File 8712, p. 1-30.

Mercier-Langevin, P., Dubé, B., and Fortin, D., 2021. Le camp minier Doyon-Bousquet-LaRonde – Aperçu historique et géologique d'un camp exceptionnel; Magazine Ressources et Industrie – Mines, v. 7, no. 1, p. 46-63.

Monecke, T., Mercier-Langevin, P., Dube, B., and Frieman, B.M., 2017. Geology of the Abitibi greenstone belt; Reviews in Economic Geology, v. 19, p. 7–49.

Nadim, L.-M. 2007. Caractérisation pétrographique et géochimique des altérations et des minéralisations aurifères de la Zone B, propriété Ellison, camp minier Doyon-Bousquet-LaRonde. Unpublished B.Sc. Thesis, Laval University, 40 p.

Osisko Mining Inc., 2021. Windfall Project; Osisko Mining Inc. < https://www.osiskomining.com/projects/windfall/> [accessed November 13, 2021].

Pacey, A., Wilkinson, J., Boyce, A., and Cooke, D., 2016. Propylitic alteration and metal mobility in porphyry systems: a case study of the Northparkes Cu-Au deposits, NSW, Australia; Applied Earth Science, v.125, p. 93.

Perry, H.K.C., Mareschal, J.-C. and Jaupart, C., 2006. Variations of strength and localized deformation in cratons: The 1.9 Ga Kapuskasing uplift, Superior Province, Canada; Earth and Planetary Science Letters, v. 249, p. 216-228.

Robert, F., 1989. Internal structure of the Cadillac tectonic zone southeast of Val d'Or, Abitibi greenstone belt, Quebec; Canadian Journal of Earth Sciences, v. 26, p. 2661-2675.

Ross, P.-S. and Bédard, J.H., 2009. Magmatic affinity of modern and ancient subalkaline volcanic rocks determined from trace-element discriminant diagrams; Canadian Journal of Earth Sciences, v. 46, p. 823-839.

Sillitoe R.H., Hannington M.D., and Thompson, J.F.H., 1996. High sulfidation deposits in the volcanogenic massive sulfide environment; Economic Geology, v. 91, p.204-212.
Sinclair, W. D., 2007. Porphyry deposits; *in* Special Publication 5; Geological Association of Canada, p. 223-243.

Stone, W.E., 1990. Archean volcanism and sedimentation in the Bousquet gold district, Abitibi greenstone belt, Quebec: implications for stratigraphy and gold concentration; Geological Society of America Bulletin, v. 102, p.147-158.

Thurston, P.C., Ayer, J.A., Goutier, J. and Hamilton, M.A., 2008. Depositional gaps in Abitibi Greenstone Belt stratigraphy: A key to exploration for syngenetic mineralization; Economic Geology, v. 103, p. 1097-1134.

Törmänen, T.O., and Koski, R.A., 2005. Gold enrichment and the Bi-Au association in pyrrhotite-rich massive sulfide deposits, Escabana trough, southern Gorda Ridge; Economic Geology, v. 100, p. 1135−1150.

Tourigny, G., Hubert, C., Brown, A.C., and Crépeau, R., 1988. Structural geology of the Blake River at the Bousquet mine, Abitibi, Quebec; Canadian Journal of Earth Sciences, v. 25, p. 581–592.

Tourigny, G., Brown, A.C., Hubert, C., and Crépeau, R., 1989a. Synvolcanic and syntectonic gold mineralization at the Bousquet mine, Abitibi greenstone belt, Quebec; Economic Geology, v. 84, p. 1875–1890.

Tourigny, G., Hubert, C., Brown, A.C., and Crépeau, R., 1989b. Structural control on gold mineralization at the Bousquet mine, Abitibi, Quebec; Canadian Journal of Earth Sciences, v. 26, p. 157–175.

Tourigny, G., Hubert, C., Brown, A.C., Crépeau, R., Trudel, P., Hoy, L., and Kheang, L., 1992. Géologie de la mine Bousquet; Ministère de l'Énergie et des Ressources du Québec, ET 89-09, 99 pages.

Tooth, B., Brugger, J., Ciobanu, C., and Liu, W., 2008. Modeling of gold scavenging by bismuth melts coexisting with hydrothermal fluids; Geology, v. 36, p. 815−818.

Valliant, R.I., and Barnett, R.L. 1982. Manganiferous garnet underlying the Bousquet gold orebody, Quebec: metamorphosed manganese sediment as a guide to gold ore; Canadian Journal of Earth Sciences, v. 19, p. 993–1010.

Valliant, R.I., and Hutchinson, R.W., 1982. Stratigraphic distribution and genesis of gold deposits, Bousquet region, Northwestern Quebec; Geology of Canadian Gold Deposits, Special Volume 24, p.27–40.

Valliant, R.I., Mongeau, and C., Doucet, R., 1982. The Bousquet pyritic gold deposit, Bousquet region, Quebec: descriptive geology and preliminary interpretations on genesis; Geology of Canadian Gold Deposits, Special Volume 24, p.41–49.

Valliant, R.I., Barnett, R.L., and Hodder, R.W., 1983. Aluminium silicate-bearing rock and its relation to gold mineralization; Bousquet mine, Bousquet township, Quebec; CIM Bulletin, v. 76, p. 81-90.

Wallbridge Mining Company Limited, 2021. Fenelon Gold Project; Wallbridge Mining Company Ltd. < https://wallbridgemining.com/our-projects/fenelon-gold/ > [accessed January 13, 2021].

Williams, N.C. and Davidson, G.J., 2004. Possible submarine advanced argillic alteration at the Basin Lake prospect, western Tasmania, Australia; Economic Geology, v. 99, p. 987–1002.

Winchester, J.A. and Floyd, P.A., 1977. Geochemical discrimination of different magma series and their differentiation products using immobile elements; Chemical Geology, v. 20, p. 325–343.

Wright-Holfeld, A., Mercier-Langevin, P., and Dubé, B., 2010. Contrasting alteration mineral assemblages associated with the Westwood deposit ore zones, Doyon-Bousquet-LaRonde mining camp, Abitibi, Quebec; Geological Survey of Canada, Current Research Paper, CR2010-9, 24 pages.

Wright-Holfeld, A., Mercier-Langevin, P., and Dubé, B., 2011. Mass changes and element mobility associated with the Westwood deposit ore zones, Doyon-Bousquet-LaRonde mining camp, Abitibi, Quebec; Geological Survey of Canada, Current Research Paper, CR2011-8. 15 pages.

Yergeau, D., 2015. Géologie du gisement synvolcanique aurifère atypique Westwood, Abitibi, Québec; Ph.D. thesis, Institut national de la recherche scientifique. – Centre Eau, Terre et Environnement, Québec, Quebec, 643 pages.

Yergeau, D., Mercier-Langevin, P., Dubé, B., Malo, M., and Savoie, A., 2022a. The Westwood deposit, southern Abitibi greenstone belt, Canada: An Archean Au-rich polymetallic magmatic-hydrothermal system - Part 1. Volcanic architecture, deformation, and metamorphism; Economic Geology, DOI 10.5382/econgeo.4878.

Yergeau, D., Mercier-Langevin, P., Dubé, B., McNicoll, V., Jackson, S. E., Malo, M., and Savoie, A., 2022b. The Westwood deposit, southern Abitibi greenstone belt, Canada: An Archean Au-rich polymetallic magmatic-hydrothermal system – Part 2. Hydrothermal alteration, mineralization, and geological model; Economic Geology, DOI 10.5382/econgeo.4879.

Table 1. Summary of the principal characteristics of the LaRonde Zone 5 and Ellison zone A and B mineralized corridors.

	LZ5 Zone 4.1	LZ5 Zone 4	LZ5 Zone 5	Ellison Zone A	Ellison Zone B
Mineralization styles	Sulfide veins, stockworks and disseminations (Py > Cpy > Sp > Po)	Sulfide veins, stockworks and disseminations (Py > Cpy > Sp > Po)	Sulfide veins, stockworks and disseminations (Py > Cpy > Sp > Po)	Disseminated sulfide with local sulfide veins, stockworks, and semi-massive to massive sulfide (Py > Cpy > Sp > Po)	Sulfide veins, stockworks and disseminations with local semi-massive sulfide (Py > Cpy > Sp > Po)
Host units	5.1a-(a), 5.1a-(b)	5.1a-(a), 5.1a-(b)	5.1a-(a), 5.1a-(b)	Ellison intermediate volcanic unit	5.3a-(b)
Thickness of the ore zones	Up to 3 m	Up to 4 m	Up to 35 m	Up to 4.5 m	Up to 6 m
Extent of mineralized zones	Hard to estimate due to lack of drilling towards the east of the LZ5 and discontinuity of ore zone	600 m along strike (east-west), but not as continuous compared to Zone 5	600 m along strike (east-west), continuous	400 m along strike (east-west), continuous	400 m along strike (NW-SE), continuous
Major minerals	Pyrite	Pyrite	Pyrite	Pyrite	Pyrite
Accessory minerals	Chalcopyrite, sphalerite, pyrrhotite	Chalcopyrite, sphalerite, pyrrhotite	Chalcopyrite, sphalerite, pyrrhotite	Chalcopyrite, sphalerite, pyrrhotite	Chalcopyrite, sphalerite, pyrrhotite
Trace minerals	Ilmenite, electrum	Ilmenite, electrum	Ilmenite, electrum	Pb and Bi rich tellurides, electrum	Galena, silver tellurides, electrum
Typical Au grades	~ 1–1.5 g/t Au over 1 m intervals, on average	~ 1–1.5 g/t Au over 1 m intervals, on average	~ 2 to 3 g/t Au for the south and north parts versus ~1 g/t Au for the central part, on average	~4–6 g/t Au over 1 m intervals, on average	~3–4 g/t Au over 1 m intervals, on average
Au/Ag ratio	No Ag data	2:1 (limited Ag data)	2:1 (based upon 2020 mill data)	1:1	1:4
Typical alteration assemblages of ore zones	Sericite-carbonate-chlorite-pyrite-quartz-feldspar-biotite	Sericite-pyrite-quartz (meter scale alteration corridor typical of Zone 4)	Sericite-carbonate-chlorite-pyrite-quartz-feldspar-biotite ± epidote	sericite-carbonate-chlorite-pyrite-quartz-feldspar	sericite-quartz-biotite ± feldspar-chlorite

Table 2. Calculated mass changes for the LZ5 and Ellison ore zones altered host rocks. Major oxides are shown in wt % while trace elements are in ppm.

	Average	Minimum	Maximum
Zr	0.0	0.0	0.0
Hf	9.7	0.0	146.7
Nb	11.6	0.1	64.0
Gd	13.4	0.0	80.9
Sm	13.7	0.0	80.3
Ga	14.4	0.0	102.0
Yb	14.7	0.0	83.6
Tb	14.9	0.1	104.5
Tm	15.2	0.1	93.8
Lu	15.5	0.1	80.1
Total	15.7	0.1	116.5
Nd	15.8	0.3	97.6
Er	15.8	0.3	108.1
SiO_2	16.3	0.0	89.3
Dy	16.4	0.0	117.9
Ho	16.6	0.0	117.5
P_2O_5	17.2	0.0	164.4
TiO_2	17.2	0.0	90.4
Y	17.3	0.1	118.5
Pr	17.6	0.1	126.4
Al_2O_3	18.2	0.2	105.8
Eu	18.7	0.0	87.4
Ce	19.2	0.0	161.9
Sc	19.6	0.0	107.1
La	20.9	0.3	163.9
U	26.3	0.2	221.1
Th	26.3	0.1	252.4
V	33.1	0.3	119.7
MgO	39.1	0.1	358.4
CaO	42.0	0.0	199.0
Cs	42.2	0.1	227.5
FeO	50.0	1.4	356.8
Co	54.0	0.0	1110.3
Li	56.8	0.4	173.3
Ta	63.6	0.2	679.1
Ba	65.0	0.1	534.1
Sr	71.3	0.2	415.5
Na_2O	75.4	1.7	278.8
$Fe_2O_3^{(t)}$	82.3	0.1	2490.7
MnO	87.9	0.1	1527.3
Ni	89.0	0.5	2237.4
Cr	107.2	0.3	6363.9
Tl	119.3	0.0	804.5
LOI	160.6	3.7	1055.6
Rb	165.6	0.6	710.8
K_2O	184.0	0.5	679.0
CO_2	650.1	9.3	3900.0
S	1700.8	0.6	31548.8